

On magnetic reconnection regimes and associated three-dimensional asymmetries: Hybrid, Hall-less hybrid, and Hall-MHD simulations

H. Karimabadi,¹ D. Krauss-Varban,^{1,2} J. D. Huba,³ and H. X. Vu¹

Received 15 March 2004; revised 1 June 2004; accepted 15 July 2004; published 22 September 2004.

[1] Magnetic reconnection in a plane current sheet is investigated in both two and three dimensions, using three different types of simulation codes, Hall MHD, hybrid (electron fluid, kinetic ions), and a new code called Hall-less hybrid. The latter code, which is similar to the hybrid code but has the Hall term removed, enables us to clarify the differences between kinetic ion and Hall MHD approaches. The major findings of this research are (1) Sweet-Parker regime of reconnection cannot be maintained and does not reach a steady state in a kinetic plasma for physically interesting parameter regimes. (2) Fast asymptotic reconnection rate of $0.15 V_{A0} B_0$ is obtained both in the hybrid and Hall-less hybrid simulations with outflow boundaries. V_{A0} and B_0 are the Alfvén velocity and magnetic field strength in the upstream region. This finding has two immediate implications. First, ion kinetics are sufficient to lead to fast reconnection even in the absence of the Hall term, and second, explanation of fast reconnection in terms of quadratic dispersion of whistlers needs to be reconsidered, as whistlers are dispersionless in Hall-less hybrid limit. (3) Unlike in MHD, diffusion region is different in size that the region of localized resistivity. (4) While both Hall and hybrid codes show that reconnection is inherently asymmetric in three dimensions, there are differences in the nature of the asymmetry. In Hall MHD we show that the X-line grows in the direction of the electron drift, propagating as a (reconnection) wave because the current is carried by electrons, although the wave direction can change in the presence of a substantial ion flow. However, in the hybrid simulations here, as is the case for typical conditions at the magnetopause and magnetotail, ions carry the bulk of the current, and the observed asymmetry is found to be due to ion flow and not a wave motion unless the extent of finite resistivity in the third dimension is very thin, comparable to the current sheet thickness. Thus aside from scenarios where electrons are the dominant current carriers, such as very thin current sheets that are on electron scales, we do not expect the reconnection wave to form. This result is relevant to the magnetotail where dawn-dusk asymmetries are observed in the motions of auroral brightenings and surges, as well as in the statistical location of pressure decreases, flows, and magnetic signatures associated with the near-Earth neutral line and early plasmoids. We attribute the observed dawn-dusk asymmetries to ion flows. One interesting question left for future work is the possibility that reconnection waves may form in thin electron-scale current layers that are sometimes observed embedded within a thicker sheet in the magnetotail. *INDEX TERMS:* 7835 Space Plasma Physics: Magnetic reconnection; 7843 Space Plasma Physics: Numerical simulation studies; 7827 Space Plasma Physics: Kinetic and MHD theory; *KEYWORDS:* 3-D reconnection, Hall-less hybrid, Hall MHD, Sweet-Parker, diffusion region, dawn-dusk asymmetry

Citation: Karimabadi, H., D. Krauss-Varban, J. D. Huba, and H. X. Vu (2004), On magnetic reconnection regimes and associated three-dimensional asymmetries: Hybrid, Hall-less hybrid, and Hall-MHD simulations, *J. Geophys. Res.*, *109*, A09205, doi:10.1029/2004JA010478.

¹Department of Electrical and Computer Engineering, University of California, San Diego, La Jolla, California, USA.

²Also at Space Sciences Laboratory, University of California, Berkeley, Berkeley, California, USA.

³Plasma Physics Division, Naval Research Laboratory, Washington, DC, USA.

1. Introduction

[2] Magnetic reconnection is an important energy conversion process [Dungey, 1961; Vasyliunas, 1975] that occurs in a variety of settings such as planetary magnetospheres, the Sun, and astrophysical plasmas. The theoretical studies of this process have focused mainly on the two-dimensional steady state solutions. The two most discussed

models of reconnection are those of Sweet-Parker [Sweet, 1958; Parker, 1957] and Petschek [1964]. The Sweet-Parker model yields reconnection rates that are too slow to explain fast dissipative events. An alternative model, with a much faster reconnection rate, was put forth by Petschek [1964], who argued that in a collisionless plasma the dissipation can occur over a small region called the diffusion region. The energy conversion is primarily achieved in this model through slow shocks that bound the reconnection region. In effect, the Petschek model consists of a Sweet-Parker current sheet that is confined to a small region, with slow shocks attached. The questions of which model is attainable and under what conditions have been the subject of much study but are still not fully understood.

[3] This issue is not just a mere theoretical curiosity but has important implications for dayside reconnection, sub-storm evolution in the magnetotail, and solar flares, among others. Most studies of the steady state reconnection have been based on two-dimensional MHD simulations [Ugai and Tsuda, 1977; Scholer, 1989; Yan et al., 1992; Ugai, 1999]. These studies have shown that Sweet-Parker reconnection is obtained unless the resistivity is localized in a small region. A more recent study by Erkaev et al. [2000], using a combination of analytical theory and simulations in an incompressible plasma, has confirmed this conclusion. They derived a generalized analytical expression for the reconnection rate as a function of the ratio of the size of the diffusion region compared with the length of the reconnection layer (system size). Their expression incorporates both Sweet-Parker and Petschek regimes as special cases. When the resistivity scale length is large and comparable to the length of the reconnection layer, the Sweet-Parker process results, independent of the magnitude of the resistivity, whereas in the limit where the resistivity is localized to a small region, Petschek-type reconnection is obtained. Biskamp and Schwarz [2001] examined the effect of localization of the resistivity and showed that the reconnection rate depends only weakly on the value of the resistivity η at the X-point and is proportional to $1/|\log \eta|$. Shay et al. [1999] classified the type of reconnection possible based on the ratio of δ/Δ , where δ is the resistivity-dependent width of the diffusion region and Δ is the length of the diffusion region along the outflow direction. Sweet-Parker is obtained if $\delta/\Delta \ll 1$ and Petschek if $\delta/\Delta \lesssim 1$. Laboratory experiments seem to favor Sweet-Parker reconnection [Uzdensky et al., 1996; Ji et al., 1999], but the small size of the plasma device in such experiments may affect the results.

[4] The above MHD-based studies have been very useful in developing an understanding of the relationship between the size of the diffusion region and the resulting reconnection geometry. However, one important question left unanswered is whether the above results hold in the kinetic regime. To address this issue, we focus our study here on three interrelated questions: (1) Do the two reconnection regimes exist and form based on the conditions stated above? (2) Do three-dimensional effects impact the results? (3) Can ion kinetics alone and in the absence of the Hall term lead to fast Petschek-like reconnection?

[5] We used hybrid (electron fluid, kinetic ions) simulations to perform a systematic study of the structure of the reconnection layer as a function of spatial extent of the resistivity in both two and three dimensions. We have also

developed a version of the hybrid code where we can remove the Hall term from the equations. This so-called Hall-less hybrid code enables us to assess the relative role of Hall effects compared with kinetic effects in our results. The results of this study have revealed a number of surprises. For instance, unlike previous studies based on resistive MHD, we find that the Sweet-Parker regime of reconnection cannot be maintained and does not reach a steady state in a kinetic plasma. Another surprising finding is the relative importance of the Hall term and kinetic effects. It is known that the Hall term plays a dominant role in the reconnection process, leading to fast reconnection as well as generation of the quadrupole structure. However, we find here that ion kinetics are sufficient to lead to fast reconnection even in the absence of the Hall term. Furthermore, the observed asymmetries in the magnetic field arising in three-dimensional (3-D) Hall-MHD simulations of reconnection [Huba and Rudakov, 2004; Shay et al., 2003] can be different in the kinetic regime. These findings, together with the fact that even the quadrupole magnetic structure can be generated solely based on kinetic effects [Karimabadi et al., 2004] even in the absence of the Hall term, indicate the importance of ion kinetics in the reconnection process.

[6] The remainder of this paper is organized as follows. Section 2 describes the simulation models. Section 3 shows the effect of spatial variations in resistivity using hybrid simulations, both 2-D and 3-D results. The summary and conclusion follow in section 4.

2. Simulation Models

2.1. Hybrid Code

[7] The basic description of various electromagnetic hybrid algorithms can be found in the work of Winske et al. [2003]. We implemented and tested the predictor-corrector, CAM-CL, and one-pass algorithms for the problem of reconnection. We found that a modified version of the one-pass algorithm (see Appendix A) has overall numerical properties comparable to the predictor-corrector algorithm but superior to CAM-CL, and we used it for all the production runs reported here. In a few cases we also used the other algorithms for comparison to ensure that the results are not modified significantly due to the choice of the algorithm. The simulation setup and normalization are the same as those used by Karimabadi et al. [1999, 2003a]. The system is initialized according to the Harris equilibrium with a background population of ions having a uniform density and with a temperature equal to the current carrying ions. The coordinate system used is such that the main component of the magnetic field is in the $\pm y$ -direction with spatial variations in the x -direction, and the current supporting this field is in the z -direction. All boundaries have freely floating field conditions that allow the magnetic field to slip as necessary. Likewise, for the ions the boundaries are of free inflow-outflow type. Escaping ions are replaced with new ions such that the first two moments are approximately constant over time, in each cell [Krauss-Varban et al., 1999a; Karimabadi et al., 1999]. In addition, the current-carrying ions are injected with the proper drift speed, as required by the Harris equilibrium, at small z for the 3-D runs. The presence of the background population gives rise to the ion-ion kink instability [Karimabadi et al., 2003b] in the plane perpendicular to

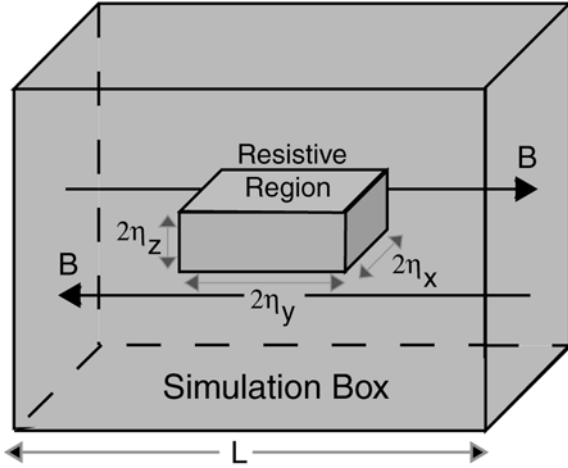


Figure 1. Schematic of the region of localized resistivity in the hybrid simulations. See color version of this figure in the HTML.

the reconnection plane. Thus in our 2-D reconnection simulations the ion-ion kink instability will not be present, but it will be present in our 3-D simulations. For details regarding the linear and nonlinear of ion-ion kink instability and its relation to the Kelvin-Helmholtz we refer the reader to *Karimabadi et al.* [2003a, 2003b].

[8] The typical simulation parameters for the 2-D runs are $\Delta x = \Delta y = 0.1 c/\omega_{pi}$, 100 particles per cell on average, and $\Omega_{ci}\Delta t = 0.001 - 0.01$. Here ω_{pi} is the ion plasma frequency and Ω_{ci} is the ion gyrofrequency. Ion plasma frequency is normalized with respect to maximum current sheet density. Other parameters include $\rho_i/L = 0.8$ and $T_e/T_i = 0.2$, where ρ_i is the ion gyroradius and L is the current sheet half thickness. The same parameters are used for the 3-D runs except the simulation box typically has $80 \times 100 \times 80$ cells, a cell size of $\Delta x = \Delta y = \Delta z = 0.25 c/\omega_{pi}$, and 60 particles per cell on average. The coordinate system is the same as in the 2-D simulations, with z being the third dimension, i.e., in the direction of the current. The time step is $0.02 \Omega_{ci}^{-1}$ or smaller, with a total run time of typically 2000 to 10,000 steps. As in the 2-D simulations, there are two ion species and electrons.

[9] The hybrid code algorithm has very little intrinsic diffusion and does not allow for reconnection unless a finite resistivity (usually localized) is set to break the frozen-in condition of the electrons. In the presence of a uniform resistivity throughout the simulation box, diffusion of the current sheet will dominate and no significant reconnection will occur unless (1) an externally imposed perturbation is introduced or (2) if there exists inherent inhomogeneities in the problem (e.g., curved magnetopause).

[10] Here we use two models for the imposed resistivity to obtain reconnection. The first is the box model, where the resistivity has a finite value of η only within a box centered in the simulation domain and having widths of $2\eta_x$, $2\eta_y$, and $2\eta_z$ in the x , y , and z directions as shown in Figure 1. In the remainder of this paper, when we refer to uniform resistivity model, we refer to this box model where resistivity has a finite and uniform value within a specified region rather than throughout the simulation domain. The second model consists of a resistivity of the form $\eta[\cosh((x - x_c)/\eta_x) \cosh$

$((y - y_c)/\eta_y) \cosh((z - z_c)/\eta_z)]^{-1}$, where the subscript c indicates the simulation domain center. By varying η_x , η_y , and η_z , we can then examine the possibility of various reconnection regimes. We have made runs with the resistivity η (normalized to $4\pi/\omega_{pi}$) of 5×10^{-6} to 4×10^{-4} and have not seen much difference except that the reconnection takes longer to develop for cases with the lower value of resistivity and may have weaker signatures. In the remainder of this paper, unless otherwise specified, the normalized resistivity η is taken to be 4×10^{-4} . The resistive scale length λ_r , normalized to the ion inertial length is given by $\eta^2/\omega_p V$, where η is normalized to $4\pi/\omega_{pi}$ and V is the flow speed normalized to the speed of light. Taking V to be $0.1 - 1V_A$ (V_A is the Alfvén speed), we obtain a resistive scale length of $0.1 - 1 c/\omega_{pi}$ for $\eta = 5 \times 10^{-5}$ and $0.8 - 8c/\omega_{pi}$ for $\eta = 4 \times 10^{-4}$. Alternatively, one can estimate the anomalous collision frequency associated with the values of η used from $\eta = m_e v_{an}/n_e e^2$. We find that $v_{an} \simeq 0.01 \omega_{pi}$ for $\eta = 5 \times 10^{-6}$ and $v_{an} \simeq 0.73 \omega_{pi}$ for $\eta = 4 \times 10^{-4}$. We will discuss the rationale for our choice of the resistivity scales in section 3.2.

[11] As an alternative to seeding the simulation with an initial perturbation, we have also performed simulations where we get the reconnection going through a localized resistivity and then make the resistivity uniform all throughout the simulation. We found in all such cases, for both hybrid and Hall-less hybrid, that once fast reconnection proceeds, the change in resistive scale length has no major effect on the subsequent evolution of the system. This is different than in MHD where the reconnection regime can change by changing the extent of the resistive region.

2.2. Hall-less Hybrid Code

[12] In order to assess the relative importance of the Hall term (i.e., the $\mathbf{J} \times \mathbf{B}$ term in Faraday's law) compared with kinetic effects, we have devised a scheme to take out the Hall term in the hybrid code. The procedure is somewhat similar to the way one would remove the Hall term in a Hall MHD code. Our starting point is Ohm's law:

$$\mathbf{E} = -\mathbf{V}_e \times \mathbf{B}/c + \eta \mathbf{J} - \nabla P_e / en_e. \quad (1)$$

Rewriting this equation in terms of ion velocity moment, we obtain

$$\mathbf{E} = -\mathbf{V}_i \times \mathbf{B}/c + \mathbf{J} \times \mathbf{B}/en_e c + \eta \mathbf{J} - \nabla P_e / en_e. \quad (2)$$

In the hybrid code this electric field is used to (1) advance the magnetic field using Faraday's law,

$$\frac{\partial \mathbf{B}}{\partial t} = -c \nabla \times \mathbf{E}, \quad (3)$$

and (2) to advance the ions. For simplicity, let us ignore $\eta \mathbf{J}$ and ∇P_e in equation (2) for the moment. Then the electric field is given by

$$\mathbf{E} = -\mathbf{V}_i \times \mathbf{B}/c + \mathbf{J} \times \mathbf{B}/en_e c. \quad (4)$$

It may at first appear that eliminating the Hall effect from the hybrid algorithm is tantamount to neglecting $\mathbf{J} \times \mathbf{B}$ in equation (4). However, this would violate the momentum

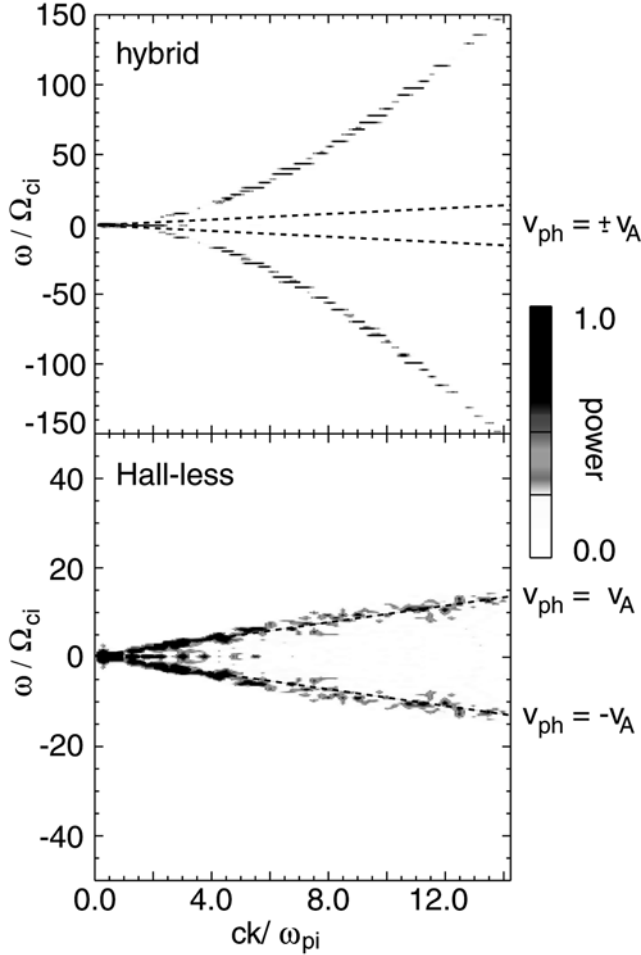


Figure 2. Whistler mode in conventional hybrid code versus Hall-less hybrid simulations, at 20° of propagation with respect to background magnetic field. The hybrid simulations exhibit the characteristic whistler dispersion, while the phase speed is nondispersive with $V_{ph} \sim V_A$ in the Hall-less case. Note difference in frequency scale; wave power units are arbitrary. See color version of this figure in the HTML.

equation. This can be seen by examining the ion momentum equation (we have neglected the pressure term for simplicity):

$$m_i \left(\frac{\partial \mathbf{V}_i}{\partial t} + \mathbf{V}_i \cdot \nabla \mathbf{V}_i \right) = en_i (\mathbf{E} + \mathbf{V}_i \times \mathbf{B}/c). \quad (5)$$

Now ignoring the Hall term in equation (4) and inserting the equation for the resulting electric field into equation (5), we see that the right-hand side of equation (5) would be identically zero. In other words, there can be no force exerted on the ions. This problem arises because the $\mathbf{J} \times \mathbf{B}/en_e c$ force is not the same as the Hall term and has to be included in the ion momentum equation. However, the Hall term can be eliminated in Faraday's law, which is used to advance the magnetic field. The magnetic field is time-advanced using equation (3) with $\mathbf{E} = -\mathbf{V}_i \times \mathbf{B}/c$ (in the code there are resistivity and pressure terms that are included but we have ignored them here for simplicity). Thus the Hall term is removed from the $\nabla \times \mathbf{E}$ term but not from the calculation of

E. This is how we proceed when removing the Hall term in the hybrid code. Consequently, the momentum equation is properly satisfied, while the Hall term is removed from the source terms of the magnetic field calculation.

[13] To illustrate the consequence of removing the Hall term in hybrid simulations, we present the dispersion relation of the wave modes for both cases in Figure 2. The graphs were obtained by Fourier-transforming perturbations in the major in-plane magnetic field component, using 2-D periodic simulations with a cell size of $0.1 c/\omega_{pi}$, a time step of $0.005 \Omega_{ci}^{-1}$, 200 by 200 cells, run for 2000 time steps with a predictor-corrector algorithm, and 4 times substepping of the magnetic field. The simulations were seeded with 4% white noise magnetic perturbations at $t = 0$, satisfying $\nabla \cdot \mathbf{B} = 0$. The evaluation is at 20° of propagation with respect to the background magnetic field, at an ion beta of 0.5 ($\beta_e = 0.05$). The wave power is plotted in arbitrary units (note the difference in frequency scale in the two panels). The conventional hybrid code (top) exhibits the characteristic whistler dispersion, while the Hall-less case (bottom) is nondispersive with a phase speed $V_{ph} \sim V_A$. We also find that the Hall-less case is typically “noisier” than the regular hybrid code when run with the same number of particles per cell. The GEM challenge study found that the Hall term is the minimum physics required for fast reconnection and explained this in terms of the quadratic nature of the whistler dispersion [Birn *et al.*, 2001; Shay *et al.*, 2001]. In the Hall-less hybrid case, however, the whistler mode is nondispersive (Figure 2), and thus one may conclude that fast reconnection may not be possible. However, as we will demonstrate shortly, not only fast reconnection is possible in the Hall-less case but details regarding the evolution of the system as a function of the diffusion region and the stability of the reconnection regimes remain similar to the full hybrid case.

[14] We emphasize that the applicability of the Hall-less hybrid code is not dependent on the relative contribution of ions and electrons to the initial current. We have used our Hall-less hybrid code for both cases where ions and electrons dominate the current, respectively. The important point is whether in the subsequent nonlinear evolution of the system the Hall term plays a dominant role over kinetic effects. The Hall-less hybrid code should be viewed as a tool for deciphering the relative role of Hall and kinetic effects in a process of interest.

2.3. Hall MHD Code

[15] The Hall magnetohydrodynamics (MHD) equations are given by

$$\frac{\partial \rho}{\partial t} + \nabla \cdot \rho \mathbf{V} = 0 \quad (6)$$

$$\frac{\partial \rho \mathbf{V}}{\partial t} + \nabla \cdot \left[\rho \mathbf{V} \mathbf{V} + (P + B^2/8\pi) \mathbf{I} - \mathbf{B} \mathbf{B}/4\pi \right] = 0 \quad (7)$$

$$\frac{\partial \mathbf{B}}{\partial t} = -c \nabla \times \mathbf{E} = \nabla \times (\mathbf{V} - \mathbf{J}/ne) \times \mathbf{B}, \quad (8)$$

where \mathbf{I} is the unit dyad and $P = nT$ where T is constant. We use the recently developed 3-D Hall MHD code VooDoo

[Huba, 2003]. VooDoo is a high-order, finite-volume code that uses a distribution function scheme to calculate the fluxes of mass, momentum, and energy at cell interfaces, as well as the convective electric field [Huba and Lyon, 1999]. The Hall electric field is updated based on an upwind scheme using high-order magnetic field values and is subcycled on the ideal MHD time scale. This scheme substantially decreases the computation time by separating the Alfvén and whistler time scales. The partial donor cell method is used to limit fluxes at sharp discontinuities [Hain, 1987]. The code uses an eighth-order spatial interpolation scheme and a second-order temporal scheme.

[16] The conditions for the 3-D simulation study are as follows. Periodic boundary conditions are used in the y direction and zero-gradient boundary conditions are used in the x and z directions ($\partial/\partial x = 0$ and $\partial/\partial z = 0$). The spatial scales are normalized to the ion inertial length (c/ω_{pi0}), the time scale to the ion gyrofrequency (Ω_{ci0}), and the velocity to the Alfvén velocity (V_{A0}) using $n = n_0$ and $B = B_0$. The equilibrium magnetic field is given by $B_y(x) = B_0 \tanh(x/x_L)$ with $x_L = 0.5$. The temperature is defined to be $C_s = V_{A0}$, where $C_s = (2T/m_i)^{1/2}$. The density profile is determined by balancing the plasma and magnetic field pressures. The maximum density is $n = n_0$ at $x = 0$ and is $n = 0.2n_0$ for $|x| > x_L$. The size of the simulation box is $L_x = 12.5$, $L_y = 26$, and $L_z = 104$. The simulations are initialized with a magnetic perturbation

$$\delta B_x = \delta B \cos(\pi x/L_x) \sin(2\pi y/L_y) F(z) \quad (9)$$

$$\delta B_y = (\delta B/2)(L_y/L_x) \sin(\pi x/L_x) \cos(\pi y/L_y) F(z), \quad (10)$$

where $F(z) = 1$ for $-26.8 < z < 20.4$ and $F(z) = 0$ otherwise. We take $\delta B = 0.02B_0$. The mesh size is $50 \times 50 \times 50$. A nonuniform stretched mesh is used in the y -direction so that there are roughly 25 grid points within the current layer. The simulations are run to time $t \simeq 46 \Omega_{ci}^{-1}$. Although there are some differences in the initial setup of the Hall and hybrid simulations, we have verified that such differences are not important in the issues that we are considering here. For example, we initialize the Hall MHD simulations by imposing a perturbation, whereas in the hybrid simulations we impose a localized resistivity to start the reconnection process. In both cases, the longer time evolution of the system beyond the initial transitory phase is insensitive to the actual method of initialization.

3. Simulation Results

3.1. Scaling With System Size

[17] In order to establish the possible role of system size on magnetic reconnection, we performed three 2-D hybrid simulations for system sizes $L_y = 50, 100,$ and $150 c/\omega_{pi}$ along the outflow direction (i.e., y -direction); all other parameters were the same. The resistivity is $\eta = 4 \times 10^{-4} 4\pi/\omega_{pi}$ within a rectangular region $\eta_x = 1 c/\omega_{pi}$ and $\eta_y = 10 c/\omega_{pi}$ and zero elsewhere. Figure 3 shows the contours of the vector potential A_z for these runs at three different times. The time evolution of the system is seen to be independent of the length of the simulation box in the y -direction. At early times, the reconnection is of the Sweet-Parker type in

all three cases. However, this configuration is not stable, as a magnetic island is seen to form due to the tearing instability, as shown in the middle panels. This island grows in time and, in the case of $L_y = 50$, fills the length of the simulation box. There are minor differences in how fast this island grows between the three cases, but the overall stability and structure of the reconnection layer are seen to be independent of the system size.

[18] In MHD there is no intrinsic scale, and thus reconnection regimes can be classified based on the size of the diffusion region compared with the system size or equivalently the length of the reconnection layer. In a kinetic plasma, however, there exist various physical scales, and ion dynamics limits and controls the rate of reconnection. Thus it is not surprising that as long as the system size is much longer than the ion inertial length c/ω_{pi} , the details of reconnection become independent of the system size. This is in agreement with the results of Shay *et al.* [1999, 2004] that showed that reconnection remains Alfvénic in a collisionless plasma even when the macroscopic scale length of the system becomes large, with a reconnection rate that is independent of the system size. They showed that the whistler induced electric field accelerates the ions to the Alfvén velocity over a spatial scale of the order $10 c/\omega_{pi}$ along the outflow direction. This illustrates the existence of a physical spatial scale in the reconnection process, and thus the details of reconnection become insensitive to the size of the system as long as L_y is sufficiently large compared with the ion inertial length.

3.2. Dependencies on the Size of Diffusion Region η_y in the Outflow Direction

[19] We saw that for the particular choice of η_x and η_y in Figure 3, a Sweet-Parker type of reconnection formed at early times but it soon evolved into a time-dependent configuration. Here we explore the role of η_y in the formation of various reconnection regimes. To this end, we have made several runs with η_y ranging from 2 to $20 c/\omega_{pi}$. Our choice for the range in the size of diffusion region considered here as measured by η_x and η_y is based on three considerations. First, there exists a physical upper bound on the size of the diffusion region in any system. In the case of magnetopause and the magnetotail, the diffusion region is much smaller than the upper bound considered here. Second, PIC simulations suggest a diffusion region much less than $20 c/\omega_{pi}$ [Pritchett, 2001], and third, it is hard to envision how the microphysics of reconnection would yield a very uniform and broad region of “resistivity” extending to many tens or hundreds of ion inertial lengths. Accordingly, we have considered a range of parameters which seem most likely to occur in a real plasma.

[20] We show in Figure 4 a contour plot of A_z from four 2-D hybrid simulations which illustrate the major points of this parameter study. The first two simulations use a box-shaped resistivity with $\eta_y = 2 c/\omega_{pi}$ and $6 c/\omega_{pi}$, respectively, and the other two simulations use the same η_x and η_y but use the “cosh shaped” resistivity profile. We use $\eta_x = 1 c/\omega_{pi}$ in all four simulations. Several conclusions can be immediately drawn from Figure 4. First, the Sweet-Parker segment of the reconnection rapidly develops into a single x -line Petschek regime for the case with a box-shaped resistivity and $\eta_y = 2 c/\omega_{pi}$, whereas the case with $\eta_y = 6 c/\omega_{pi}$ becomes time-

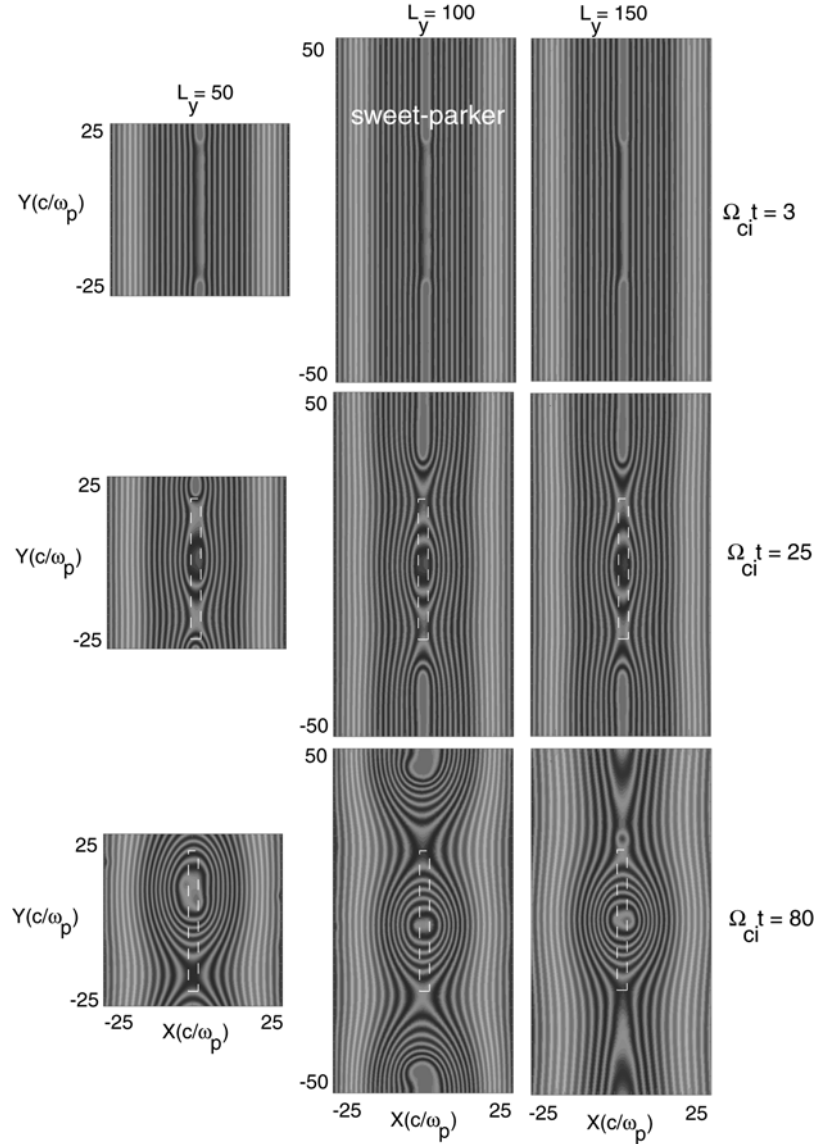


Figure 3. Two-dimensional (2-D) hybrid simulations. Contour plots of the vector potential A_z for three runs differing only in the size of the box in the y -direction. See color version of this figure in the HTML.

dependent. The transition point between these two distinct solution is at $\eta_y \sim 4 c/\omega_{pi}$. This result differs from MHD reconnection studies [Scholer, 1989; Yan et al., 1992; Shay et al., 1999; Biskamp and Schwarz, 2001]. In MHD, Sweet-Parker reconnection is a stable configuration which will be attained when the resistivity scale length is large and comparable to the length of the reconnection layer. In the kinetic regime, the Sweet-Parker reconnection is not a steady state solution and eventually becomes unstable. Second, the reconnection appears to be Petschek-like, independent of the value for η_y when we use a cosh profile for the resistivity (e.g., see the two panels on the far right of the figure). The use of the cosh profile leads to a resistivity profile that can be thought of as a superposition of a box-shaped (uniform within a rectangular domain) resistivity and a spatially varying resistivity. This has the effect of having a small η_y which then leads to a Petschek regime. However, it is conceivable that in cases when the resistivity

η is very weak, the use of the cosh profile may give results more similar to the box-shaped resistivity cases.

3.3. Dependencies on the Size of Diffusion Region η_x in the Inflow Direction

[21] Previous studies based on MHD have typically considered a diffusion region that has the same spatial extent both in the inflow and outflow regions of reconnection. Here we examine the changes in the reconnection in the kinetic regime as a result of varying η_x . The first two columns in Figure 5 shows the contour plots of A_z at three different times for $\eta_x = 1 c/\omega_{pi}$ and $10 c/\omega_{pi}$. Note that the snapshots of the contour plots shown correspond to different times between the two cases. The first case (the three leftmost panels) is similar to what we have already observed in Figures 3 and 4, namely a Sweet-Parker regime that becomes unstable in time and the formation of a magnetic island. However, in the case where $\eta_x = 10 c/\omega_{pi}$, the Sweet-

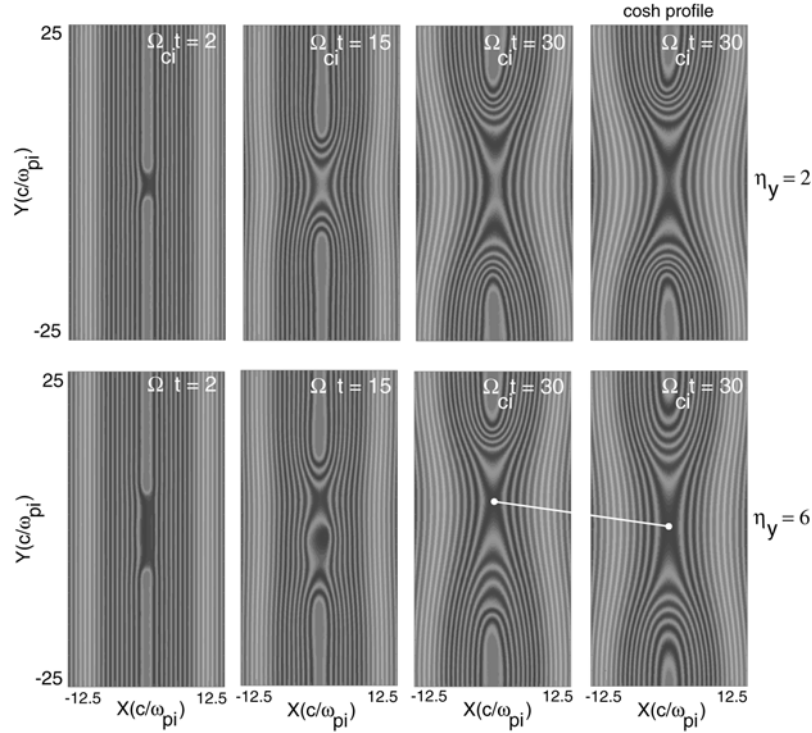


Figure 4. The 2-D hybrid simulations. Contour plots of the vector potential A_z for box shaped and cosh profile of resistivity at two different resistivity scale lengths in the y -direction of $\eta_y = 2$ and $6 c/\omega_{pi}$. $\eta_x = 1 c/\omega_{pi}$ in all cases. Reconnection reaches steady-state for cosh profile cases, whereas it becomes time dependent for box shaped resistivity profiles if $\eta_y > 3 c/\omega_{pi}$. See color version of this figure in the HTML.

Parker regime is maintained over a much longer time compared with the $\eta_x = 1 c/\omega_{pi}$ case, and rather than form a magnetic island, it transitions to a Petschek-like configuration. The three panels on the far right of Figure 3 show the results for the case where $\eta_x = 10 c/\omega_{pi}$, and $\eta_y = 1 c/\omega_{pi}$. In this case the reconnection proceeds quickly to the Petschek regime. Thus the size of η_y determines the extent of the Sweet-Parker current sheet, whereas the details of the time evolution and whether a steady state is possible in each case are controlled by a combination of both η_x and η_y .

3.4. Effect of Hall Term on the Reconnection Regimes

[22] The Hall term has long been thought to play a significant role in magnetic reconnection [Sonnerup, 1979; Terasawa, 1983; Mandt et al., 1994]. In this section we explore the possibility of whether the absence of the Hall term in MHD may be the prime factor in giving rise to the differences seen between MHD simulations and our kinetic simulations. To this end, we have performed Hall-less hybrid simulations and compared the results with the full hybrid code. The results of the Hall-less simulations are described here. Figure 6 shows contours of A_z at two different times from three different hybrid simulations. In all three cases, $\eta_x = 1 c/\omega_{pi}$, $\eta_y = 20 c/\omega_{pi}$, and the resistivity has a box shape except the panels in the last column which have a resistivity with a cosh profile. Comparing the usual hybrid simulation (first column) with the Hall-less result (middle column), we find that the absence of the Hall term allows the Sweet-Parker phase of reconnection to remain stable to longer times ($\Omega_{ci}t = 25$ rather than $\Omega_{ci}t = 4$), but it eventually becomes unstable as in the original case with the

Hall term. Thus the fact that in the kinetic regime the Sweet-Parker regime is unstable whereas in MHD it is stable is not entirely due to the Hall term. The panels in the last column are to be compared with the two panels in the first column. The results shown in these two columns are based on the standard hybrid code, which includes the Hall term, but the former has a cosh profile for resistivity. In contrast to the box shape case, the cosh profile results in a Petschek regime, with the diffusion region confined to a small region close to where η has its peak. This peak region acts like a source of enhanced resistivity, allowing reconnection to develop into Petschek regime.

[23] We have also performed a series of runs, shown in Figure 7, where we start the simulation with a small localized resistivity ($\eta_x = 1 c/\omega_{pi}$, $\eta_y = 1 c/\omega_{pi}$) and then change η_y to $L_y/2$ at $\Omega_{ci}t = 20$. Figures 7a and 7b show the field lines right before η_y is changed and at the end of the run after η_y was increased. Figure 7c shows the field lines for the case where η_y was kept constant throughout the run. The corresponding runs with the Hall term switched off in the hybrid code are shown in Figures 7d–7f. From Figure 7 we can draw two conclusions. First, reconnection proceeds slower and Petschek structure takes longer to develop in the Hall-less case. This is quantified in Figure 8, which shows the growth rates of the tearing mode (combined power in modes 1–5) in the simulations shown in Figures 7a (hybrid) and 7d (Hall-less hybrid). Although the initial configurations are identical in these two runs, the growth rate is seen to be over a factor of 2 slower in the Hall-less hybrid case. Second, after the Petschek reconnection has developed, extending the resistive region by increasing η_y , neither takes

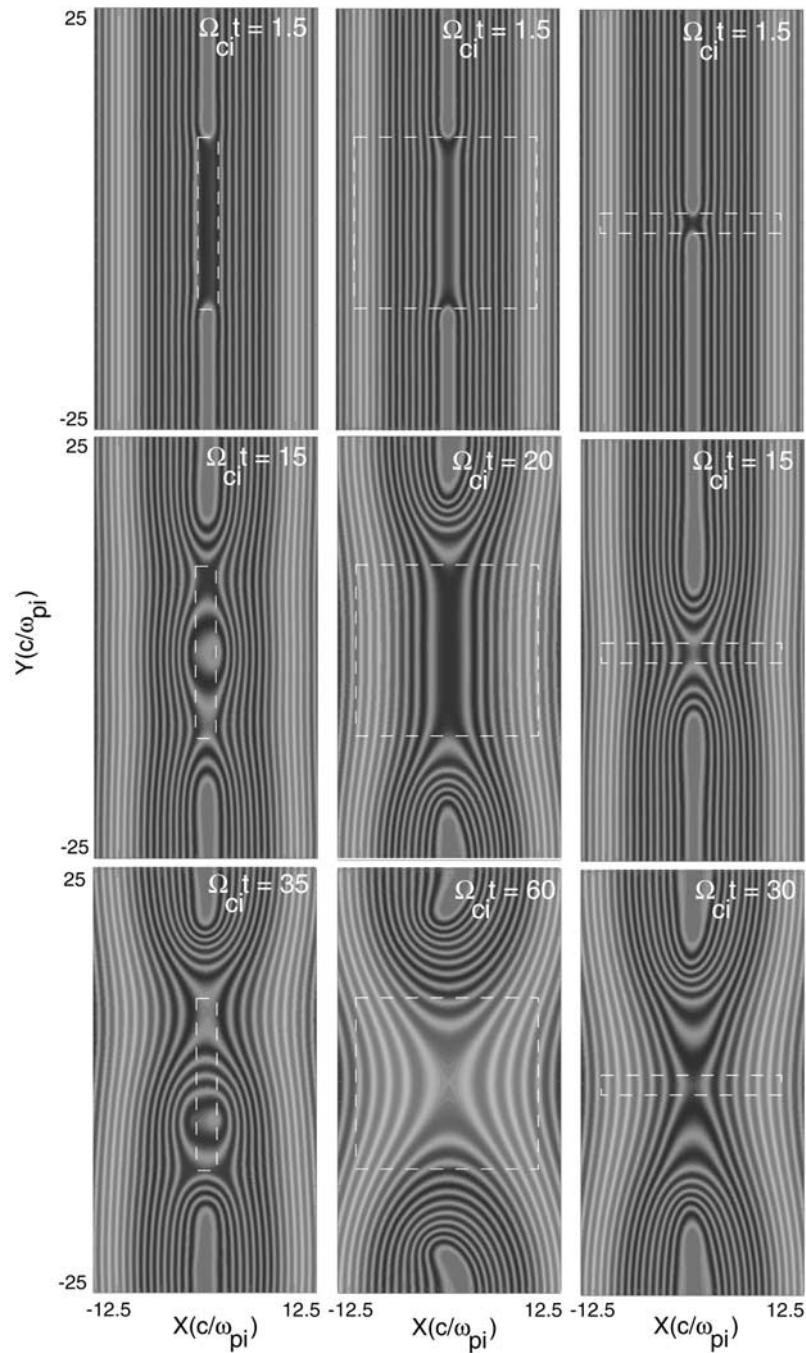


Figure 5. The 2-D hybrid simulations. Time evolution of the contour plots of the vector potential A_z for box-shaped resistivity profiles having (η_x, η_y) of (1, 10), (10, 10), and (10, 1), respectively. See color version of this figure in the HTML.

the system to Sweet-Parker regime nor does it make the system unstable. This is in contrast to MHD. For instance, *Yan et al.* [1992] found that modifying the resistivity from localized to uniform after some time destroys the Petschek structure and only a long current sheet is left, which in turn becomes unstable to the tearing mode. Another interesting result can be seen when we compare the results of the two cases where we modified the resistivity profile during the run, one with Hall term and one without, with the corresponding runs with a time stationary resistivity profile (the bottom panels in Figure 7). Apparently, modifying the

resistivity profile after Petschek reconnection has been established does little to change the reconnection structure. The only notable difference between the bottom panels and the middle panels is that the maintenance of a small η_y results in a somewhat smaller diffusion region where the x-line has formed.

3.5. Fast Reconnection Due to Ion Kinetics

[24] Reconnection rate is a useful means of quantifying the efficiency of the reconnection process, and there are various definitions of it in the literature. A detailed study of

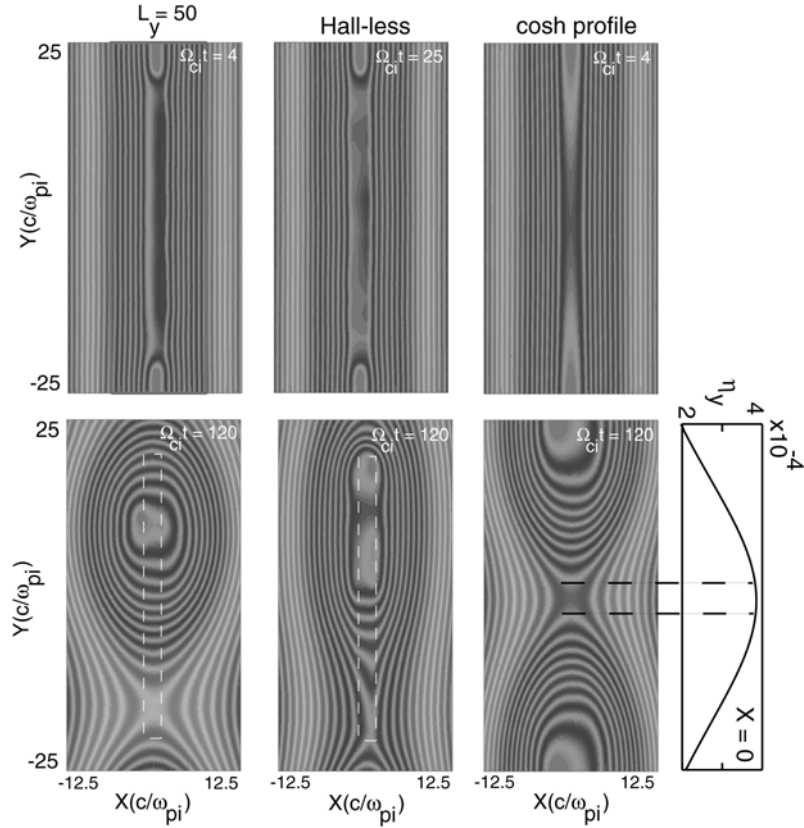


Figure 6. The 2-D hybrid simulations. Time evolution of the contour plots of the vector potential A_z for (a) box-shaped resistivity profile with $\eta_x = 1 c/\omega_{pi}$, $\eta_y = 20 c/\omega_{pi}$, (b) same as Figure 6a but with the Hall term removed in the hybrid code, (c) same as Figure 6a but with a cosh resistivity profile. See color version of this figure in the HTML.

reconnection rate will be addressed elsewhere. Here we are only interested in determining whether it is possible to have fast reconnection due to ion kinetics alone if we remove the Hall term. Let us consider the evolution of a current sheet from the onset of reconnection to its final steady state configuration. The initial phase is dominated by electron physics where the frozen-in condition is broken. The second phase involves the growth of the island or islands to ion scales, followed by the final phase where the system reaches steady state. The evolution time of the system from onset to steady state is highly dependent on the initial configuration (e.g., current sheet thickness), and the instantaneous value of the reconnection rate will vary in time until steady state is reached. In GEM challenge [Birn *et al.*, 2001; Kuznetsova *et al.*, 2001], the initial linear growth phase was bypassed by imposing a rather large external perturbation, and the reconnection rate was calculated and compared based on MHD, Hall MHD, hybrid, and full particle simulations. Since periodic simulations (in the direction along the initial magnetic field) were used, only the time-dependent reconnection rate in the second phase of the current sheet stated above could be calculated [Kuznetsova *et al.*, 2001]. In a periodic simulation the outflow jets that reach the boundary will start to come into the simulation on the opposite side. Implementation of outflow boundary condition is required to allow the system to reach steady state. In GEM challenge studies it was found that reconnection rate is insensitive to

the details of how the frozen-in condition is broken and found similar rates in Hall MHD, hybrid, and full particle simulations but found much lower reconnection rate in MHD. Fast reconnection and its absence in MHD was explained in terms of the quadratic dispersion property of whistlers (higher phase speed at smaller spatial scales).

[25] Here we take a different approach and use simulations with inflow-outflow boundary conditions to compare the asymptotic value of the reconnection rate between the hybrid and Hall-less hybrid simulations. Since whistlers are dispersionless in the Hall-less hybrid case (e.g., Figure 2), we can also test the connection between whistler dispersion and fast reconnection as suggested by GEM challenge studies. To this end, we performed two 2-D simulations, one hybrid and one Hall-less hybrid, with identical initial conditions and ran them till they reached steady state. These simulations are $30 \times 40 c/\omega_{pi}$ large, with a cell size of $0.5 c/\omega_{pi}$, and 2400 particles per cell. Resistivity is set using the \cosh^{-1} model, with a half-width of $1 c/\omega_{pi}$. It took $\sim 20\text{--}25 \Omega_{ci}^{-1}$ for both the hybrid and Hall-less hybrid runs to reach steady state. In this multicomponent plasma (equilibrium and background ions), steady state can be identified best in the outflow B_x , which starts to develop a plateau following the initial outflow plasmoid. On the other hand, other quantities such as the outflow speed may accelerate at late times, when most of the initial equilibrium ions have left the system. Since whistlers are dispersionless in the

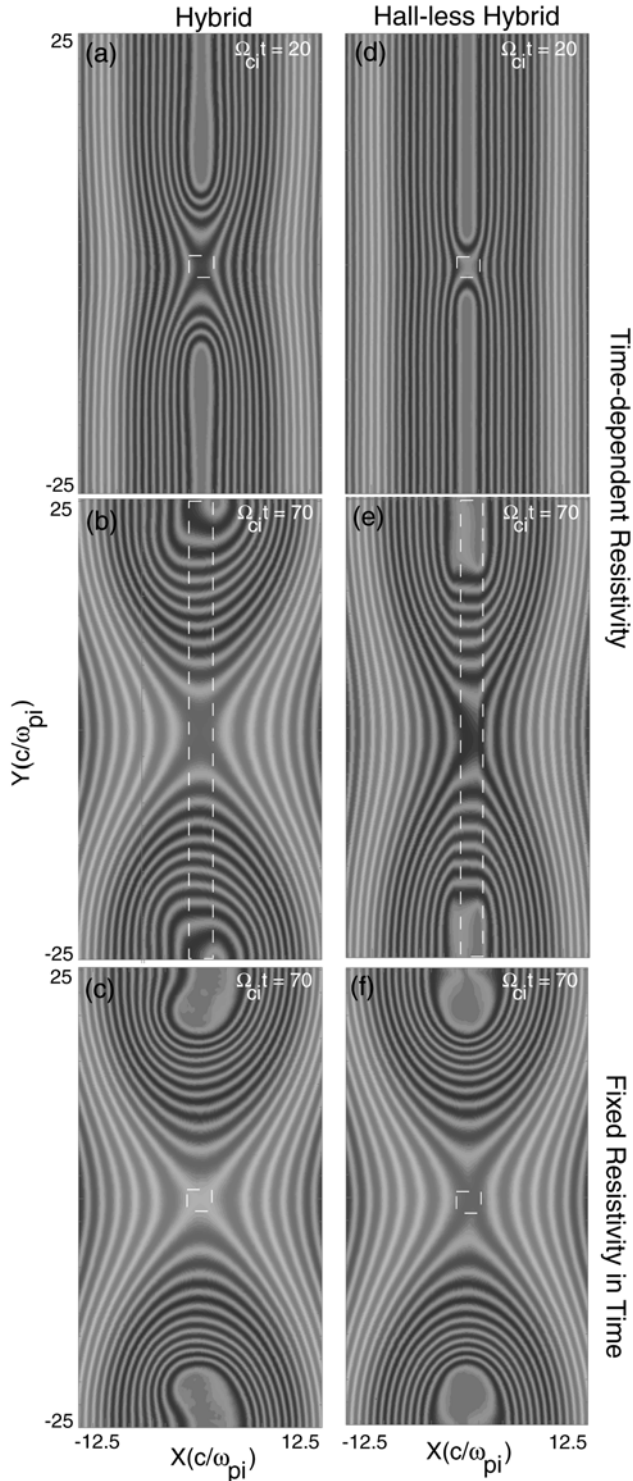


Figure 7. The 2-D hybrid simulations. Time evolution of the contour plots of the vector potential A_z : (a) box-shaped resistivity profile with $\eta_x = 1 c/\omega_{pi}$, $\eta_y = 1 c/\omega_{pi}$, (b) η_y was changed to $25 c/\omega_{pi}$ at $\Omega_{ci}t = 20$, (c) η_y was kept fixed at $1 c/\omega_{pi}$, (d)–(f) equivalent runs corresponding to Figures 7a–7d but with the Hall term removed from the hybrid code. See color version of this figure in the HTML.

Hall-less hybrid case (Figure 2), one may expect the reconnection rate to be much lower than in the hybrid case. We used the value of $V_y B_x$ (outflow), normalized to $V_{A0} B_0$, a reasonable distance away from the diffusion region as the measure of the asymptotic reconnection rate. Here, V_{A0} and B_0 are the Alfvén velocity and magnetic field strength in the upstream region. For the hybrid run, we find $V_x B_y$ (inflow) = $0.15 \sim V_y B_x$ (outflow) = 0.17 , with $V_x = 0.15$, $B_y = 1.0$, $V_y = 0.5$, and $B_x = 0.34$. For the Hall-less hybrid we find $V_x B_y$ (inflow) = $0.15 \sim V_y B_x$ (outflow) = 0.16 , with $V_x = 0.15$, $B_y = 1.0$, $V_y = 0.5$, and $B_x = 0.32$ (all in normalized simulation units). In GEM challenge study, *Kuznetsova et al.* [2001] found a peak reconnection electric field of ~ 0.25 , which lasted for a brief time before dropping to ~ 0.15 by the end of their run. This is in good agreement with the asymptotic value of ~ 0.15 found here.

[26] A detailed study of reconnection rate and its potential dependencies on initial configuration and choice of parameters will be addressed elsewhere. Thus our point of emphasis here is not on the actual value of the reconnection rate, which may or may not depend on the initial configuration and choice of parameters. Rather our goal was to determine whether there would be a significant difference in the reconnection rate between the hybrid and the Hall-less hybrid simulations. Our find that the reconnection rate is comparable in the hybrid and Hall-less hybrid simulations demonstrates two very important points: (1) ion kinetics alone can give rise to fast reconnection and (2) quadratic property of whistlers is not critical to fast reconnection in the kinetic regime.

3.6. Three-Dimensional Effects

3.6.1. Effect of η_z

[27] In this section we consider the changes in the reconnection regime when the width of the area with finite resistivity is varied in the third direction η_z . Unless otherwise mentioned, we use our standard cosh functional format, with the resistivity thus falling off quickly away from the center of the simulation domain. We will also show examples with the box shape resistivity. At first, we fix $\eta_x = \eta_y = 1 c/\omega_{pi}$ and take $\eta_z = 0.25, 1$, and $4 c/\omega_{pi}$, with the addition of a case with uniform resistivity along z . We use $\eta = 5 \times 10^{-5}$ in these runs, which translates to a diffusion length of 0.1 to $1 c/\omega_{pi}$ (using a characteristic velocity of $1.0 V_A$ to $0.1 V_A$). As we show below, such a small value on the other hand leads to fairly slow reconnection rates. For comparison, we ran the two cases with the thinnest width η_z also with four times the above standard value of η .

[28] The expectation is that reconnection becomes slower and eventually ceases when the width of finite resistivity becomes too small in z , with the natural length scale being the ion inertial length. It is for this reason that we have chosen a cell size of $0.25 c/\omega_{pi}$, which is somewhat small compared with typical 3-D hybrid simulation runs, so we can resolve dependencies in the vicinity of and just below the ion inertial length. Note that a cell size of $1 c/\omega_{pi}$ resolves waves with a wave number of $ck/\omega_{pi} \sim 3$, which is often sufficient because of strong damping of modes with $k \gtrsim c/\omega_{pi}$.

[29] Table 1 shows the results for all of our cases in terms of the strength of the maximum reconnection fields B_x and B_z , as well as the reconnection flow V_y , at $\Omega_{ci}t = 20$.

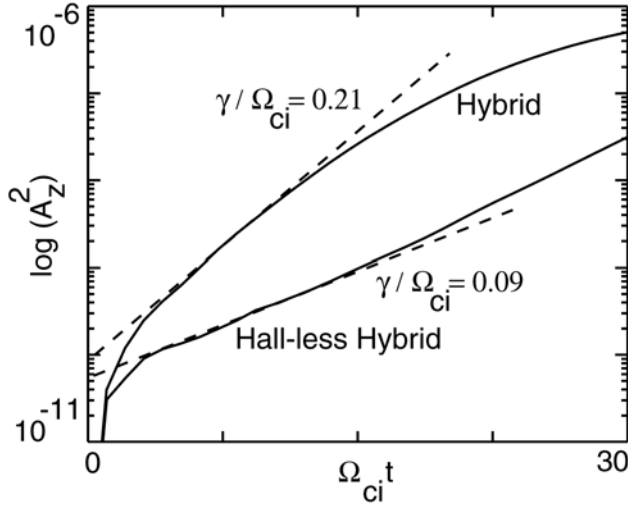


Figure 8. Growth rate of the tearing mode (combined power in modes 1–5) for the simulations shown in Figures 7a (hybrid) and 7d (Hall-less hybrid).

Typically, the values only change by about or less than 15% at twice this time (see also Figure 11 below for the temporal evolution), so it is appropriate and justified to concentrate on the early time development for our purposes. Clearly, the largest reconnection values are achieved when reconnection is pseudo 2-D, i.e., when the resistive width in z is infinite as far as the simulation is concerned. Even in the case $\eta_z = 4.0 c/\omega_{pi}$, reconnection is much less efficient than in the pseudo 2-D case. All values in Table 1 are slowly varying functions of η_z , indicating that while c/ω_{pi} is the characteristic scale where reconnection diminishes, there is no magic number at which reconnection ceases abruptly. Also, it comes as no surprise that the diffusion length scale needs to be comparable to or smaller than the ion inertial length in order to resolve this dependence on η_z (see results for $\eta = 2 \times 10^{-5}$ in Table 1).

[30] Figure 9 shows an $x - z$ cross section of the reconnected field B_x in three simulation cases with $\eta_z = 0.25 c/\omega_{pi}$, $1.0 c/\omega_{pi}$, and $4.0 c/\omega_{pi}$, respectively, at $20 \Omega_{ci}^{-1}$. The cut is taken $3 c/\omega_{pi}$ away from the center. Note that the scales are different in each case. As expected, reconnection falls off rapidly away from $z = 0$. Not only is the area in z over which reconnection takes place different in each case, scaling with η_z , but reconnection also becomes increasingly difficult for small η_z of the order of or smaller than c/ω_{pi} .

[31] Sensitivity of the reconnection process to the width in the z -direction has also been pointed out in MHD simulations [Ugai, 1999] and in a recent Hall-MHD study [Yokokawa et al., 2001]. However, Yokokawa et al. [2001] concentrate on field-aligned current patterns and the scaling with the current layer thickness, also in a somewhat different region of parameter space, so the results are not directly comparable. Here, our main finding is that while reconnection becomes increasingly inefficient for small η_z of the order of or smaller than c/ω_{pi} , this is a gradual transition that starts at $\eta_z \gg 1 c/\omega_{pi}$ and has no sharp threshold at $\eta_z = 1 c/\omega_{pi}$.

3.6.2. Asymmetric Reconnection

[32] In this section, we explore the effects arising in 3-D. As we demonstrate, both Hall MHD and hybrid simulations reveal asymmetries in the z -direction but a closer examination reveals marked differences in the origin and properties of these asymmetries.

3.6.2.1. 3-D Hall MHD

[33] The results of our Hall MHD simulation [Huba and Rudakov, 2002] are shown in Figure 10. We show greyscale contours of the plasma density and velocity vectors as a function of space (xz plane at $x = 0$) at times $t = 1.3, 14.3, 28.7,$ and 43.1 . The “white” contour corresponds to a high density, while the “black” contour corresponds to a low density. The velocity vectors are “wind flags” where the small diamond is at the base of the vector. Three observations are made. First, although the initial perturbation width is $\Delta z \simeq 6$, the reconnection layer extends a distance of $\Delta z \simeq 70$ at $t = 43.1$. Second, the reconnection site propagates asymmetrically; it only propagates in the $-z$ direction from its initial position at $z \sim -22$. The disturbance does not propagate into the region $z < -30$. And third, as the reconnection wave propagates in the $+z$ direction, plasma flows are directed not only toward the neutral line but also in the direction of the current (i.e., the $+z$ direction) at the front of the wave; this is evident at time $t = 43.1$ near $z \simeq 40$ and $x \simeq 0.5$. After the reconnection wave has passed through the system, the resulting flow pattern away from the neutral line is similar to the 2-D case, i.e., plasma flows are only directed toward the neutral line at $x = 0$. This is shown at time $t = 43.1$ in the region $-10 < z < 20$. However, at the neutral line ($x \simeq 0$ and $y \simeq 0$) there are strong flows in the $-z$ direction.

[34] The Hall term introduces new wave modes in the system, e.g., whistler waves and Hall drift waves. We now derive the dispersion equation for these wave modes and discuss them. We assume that the equilibrium magnetic field is $\mathbf{B} = B_0(x) \mathbf{e}_y$ and the plasma density is inhomogeneous in the x -direction $n = n_0(x)$. The equilibrium state is $n(T_i + T_e) + B^2/8\pi = \text{const}$. We further assume in this section that the plasma is isothermal $T_e = \text{const}$ and $T_i = \text{const}$. For simplicity we consider the collisionless EMHD limit ($\eta = 0$ and $\mathbf{V} = 0$) so that the current is maintained by the electron drift in the $-z$ -direction due to the Hall electric field $E_x = (1/en)d(nT_i)/dx$.

[35] In order to understand the asymmetric propagation of the reconnection line, we solve Faraday’s Law to obtain the Hall MHD wave modes. The magnetic field is perturbed

Table 1. Strength of the Maximum Reconnection Fields B_x and B_z As Well As the Reconnection Flow V_y , at $20 \omega_{ci}^{-1}$, For Four Different Values of the Width η_z of Finite Resistivity in z , and For Two Values of the Maximum Resistivity^a

η		$\eta_z = 0.25$	$\eta_z = 1.0$	$\eta_z = 4.0$	$\eta_z = \infty$
		c/ω_{pi}	c/ω_{pi}	c/ω_{pi}	
0.5×10^{-5}	$ B_x/B_0 $	0.10	0.16	0.18	0.45
	$ B_z/B_0 $	0.06	0.12	0.15	0.40
	$ V_y/V_A $	0.10	0.15	0.20	0.70
2.0×10^{-5}	$ B_x/B_0 $	0.22	0.25		
	$ B_z/B_0 $	0.18	0.20		
	$ V_y/V_A $	0.20	0.30		

^aNormalization is with respect to the asymptotic magnetic field B_0 and the Alfvén velocity V_A based on that and the current sheet center density.

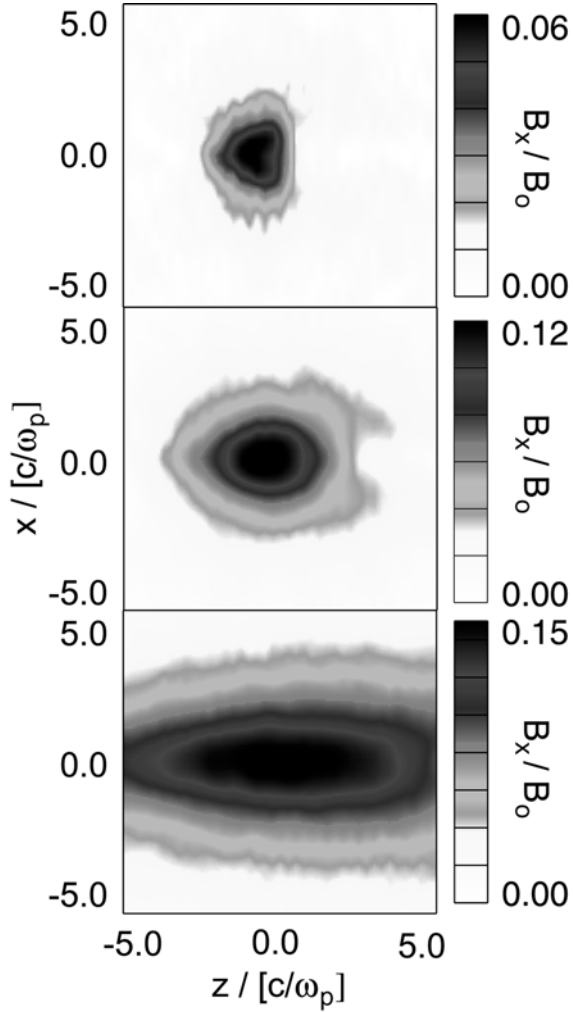


Figure 9. The $x - z$ cross section of the reconnected field B_x in three cases with $\eta_z = 0.25 c/\omega_{pi}$, $1.0 c/\omega_{pi}$, and $4.0 c/\omega_{pi}$, respectively, from top to bottom. Cut taken $3 c/\omega_{pi}$ away from the center. Note scales are different in each case. See color version of this figure in the HTML.

with $\delta B \propto \exp(ik_y y + ik_z z - i\omega t)$, and we assume the local approximation $\partial \delta B / \partial x \ll k \delta B$. The dispersion equation is

$$(\omega - k_z V_n)(\omega - k_z V_B) = k_y^2 V_A^2 (c^2 k^2 / \omega_{pi}^2), \quad (11)$$

where $k = (k_y^2 + k_z^2)^{1/2}$, $V_A = B_0 / (4\pi\rho)^{1/2}$ and

$$V_n = \frac{cB_0}{4\pi en} \frac{1}{n} \frac{\partial n}{\partial x} \quad V_B = \frac{c}{4\pi en} \frac{\partial B_0}{\partial x}.$$

[36] In the homogeneous limit ($\partial/\partial x = 0$) the whistler wave is obtained: $\omega = \pm k_y V_A (ck/\omega_{pi})$. However, in the inhomogeneous limit, two waves with different phase velocities develop. In the limit $k_y L \ll 1$, where L is the scale length of the plasma or field inhomogeneity, the wave modes are

$$\omega_1 = k_z V_n \quad \text{and} \quad \omega_2 = k_z V_B. \quad (12)$$

Because the density and magnetic field gradients are in opposite directions in the current layer, these drift modes propagate in opposite directions. We refer to the first solution $\omega = k_z V_n$ as the Hall drift wave; it corresponds primarily to the perturbation of the B_y component and propagates in the $\mathbf{B} \times \nabla n$ direction. A detailed theoretical and numerical treatment of this mode was presented by *Huba* [1991]. The second wave $\omega = k_z V_B$ propagates at the electron drift velocity and is associated with curvature of the magnetic field. Moreover, it regulates the evolution of magnetic field line reconnection in three dimensions and we refer to this wave mode as a reconnection wave [*Huba and Rudakov, 2002*]. It is important to recognize that the electrons carry the current in this analysis, since the ions are immobile. This is the situation for very thin current layers (i.e., $L \ll c/\omega_{pi}$). It is possible that if there are sufficiently strong ion flows present in the direction of the current, then the wave propagation direction could change [*Shay et al., 2003*]. In fact, we show that ion dynamics can lead to different results for thicker layers when the ions carry the current as shown in the next section.

3.6.2.2. 3-D Hybrid Simulation Results

[37] We examine the details of 3-D reconnection for the case when the half-width of the area with resistivity is fixed at $1 c/\omega_{pi}$ in all directions with a cosh profile. The value of the maximum resistivity is $\eta = 5 \times 10^{-5}$ in simulation units. Reconnection in 3-D is asymmetric in the z -direction in hybrid simulations [*Krauss-Varban and*

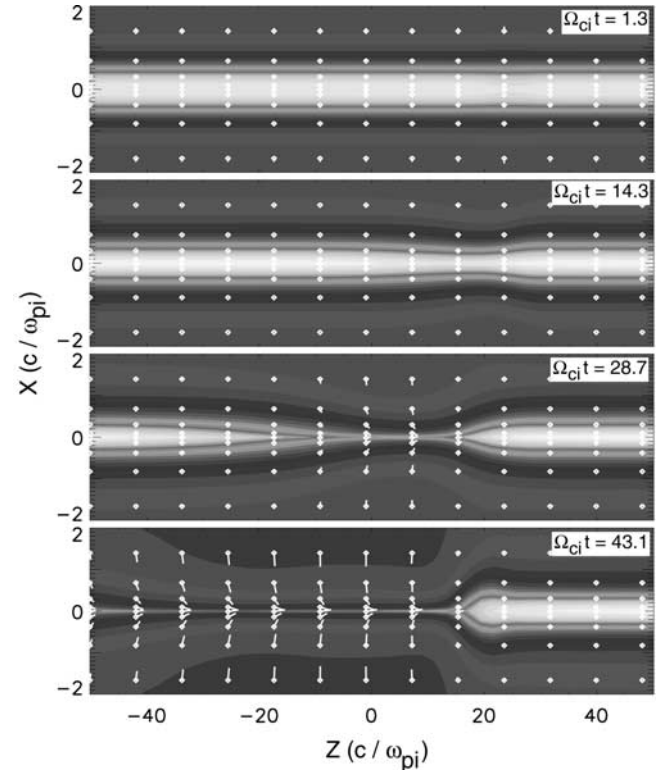


Figure 10. Contour plots of the plasma density and velocity vectors at times $t = 1.3, 14.3, 28.7, 43.1$, using the 3-D Hall MHD code VooDoo. See color version of this figure in the HTML.

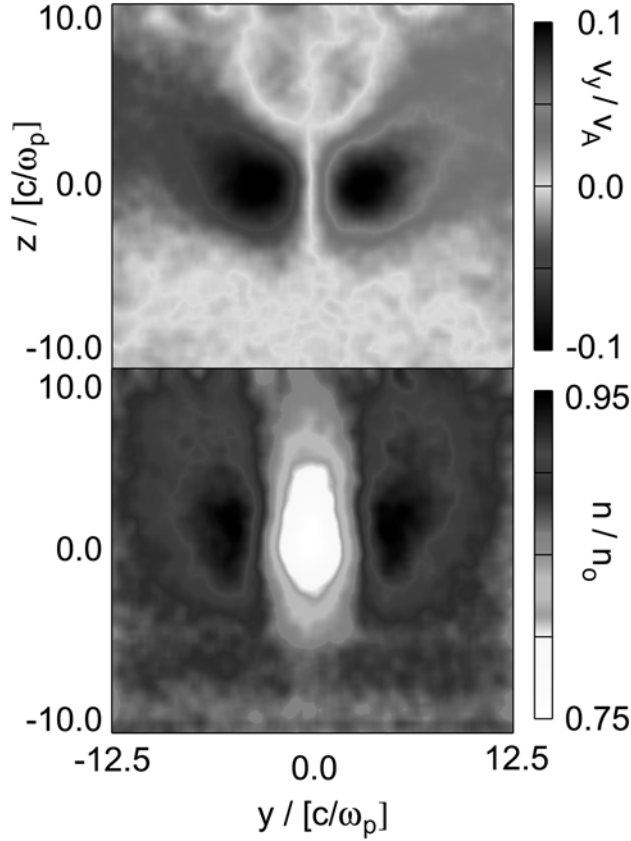


Figure 11. Normalized outflow velocity V_y and density n in $y - z$ midplane cross section at $t = 20 \Omega_{ci}^{-1}$. The results show that the reconnection signatures are transported downstream (to larger z) with the flow of the current-carrying ions. See color version of this figure in the HTML.

[Karimabadi, 2003] but in a different way than the Hall MHD results described above. When the ions carry a significant fraction of the current, the 3-D reconnection configuration is heavily affected by the motion/momentum of the current-carrying ions [Krauss-Varban *et al.*, 1999a]. Details of this depend sensitively on a number of parameters, such as the reconnection rate, η_z , and the beta of the uniform background ions. The flow of the current-carrying ions in the z -direction means that reconnection signatures, such as V_y and the density enhancement n/n_0 , are carried to larger z away from the reconnection (simulation) center. We concentrate here on the behavior at early times. Figure 11 shows these two quantities in the $y - z$ midplane cross section at $20 \Omega_{ci}^{-1}$. It is quite apparent that the reconnected plasma drifts to larger z , creating a strong asymmetry.

[38] The motion of the ions through the finite-size reconnection region also affects where reconnection can take place. Thus when the diffusion region is comparable to or larger than an inertial length, the reconnection magnetic field tends to show an asymmetry with larger reconnection signatures at larger z (see Figure 6). In addition, the z -component of the magnetic field attains a much more complicated, asymmetric pattern. This is demonstrated in Figure 12, which shows five $x - y$ cross

sections of B_z at various distances away from the simulation center, as indicated. Clearly, the strongest reconnection signature in B_z is a few c/ω_{pi} away from the center ($\sim 2.5 c/\omega_{pi}$ in this case). In addition, immediately on the upstream side of $z = 0$, the internal quadrupole signature is reversed compared with the traditional signature at larger z , which is closer to the behavior in 2-D. This reversed signature is also seen in 2-D, often at early times, and inside the region with traditional sign [Karimabadi *et al.*, 2004].

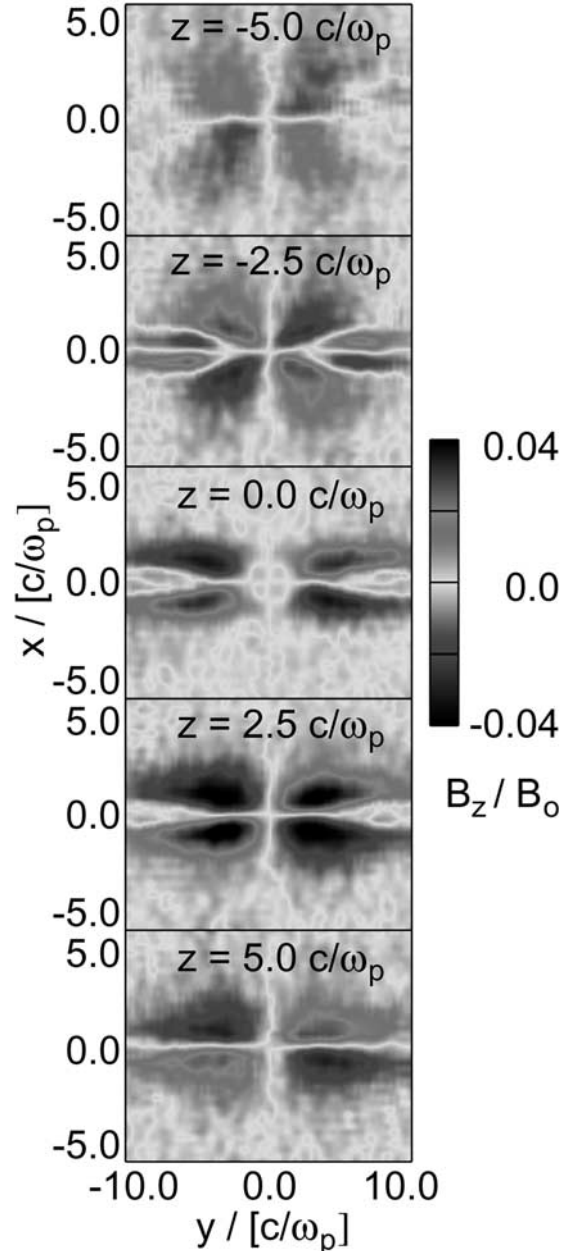


Figure 12. Magnetic field component B_z in 3-D hybrid simulations at five cross sections in the $x - y$ plane, as indicated. B_z is largest a few ion inertial lengths downstream of the diffusion region center. See color version of this figure in the HTML.

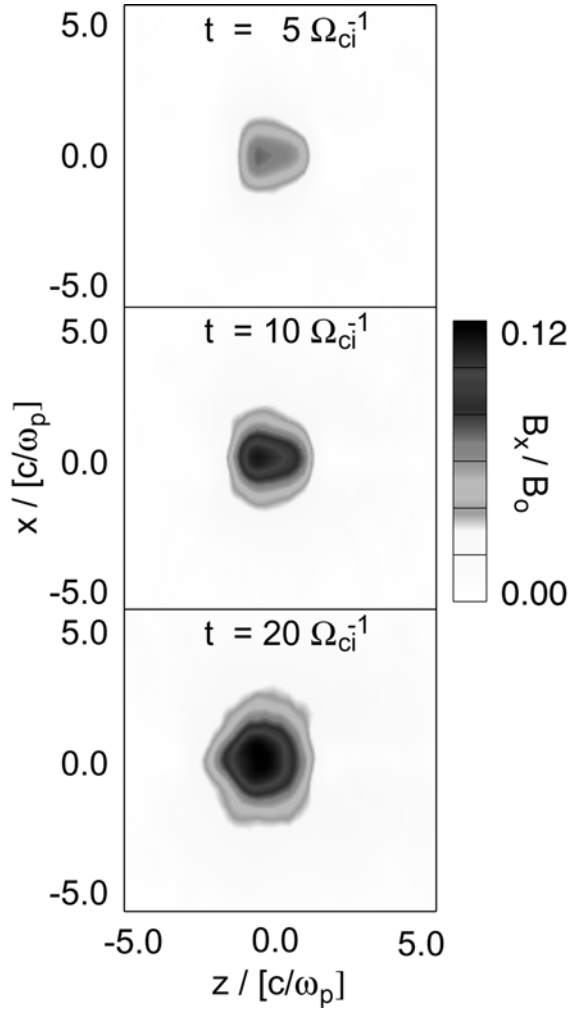


Figure 13. Evolution of the reconnection magnetic field B_x in 3-D hybrid simulations at three different times, as indicated. Results for a box profile of resistivity in the z -direction, with $\eta_z = 1.0 c/\omega_{pi}$ and $\eta = 5 \times 10^{-5}$. Reconnection quickly fills out the region with finite resistivity on both sides away from the center (along z). See color version of this figure in the HTML.

[39] As we showed in Figure 10, an asymmetric proceeding of reconnection also occurs in the 3-D Hall-MHD simulations [see also *Huba and Rudakov, 2002*]. Similar to our setup in the hybrid simulation, reconnection is started in a finite-sized region along z . However, different from the hybrid simulations, reconnection in Hall-MHD can in principle proceed everywhere and is not limited to a region of finite resistivity. In such Hall-MHD simulations, enhanced reconnection initially propagates as a wave front in the direction opposite to the current. This asymmetry is due to a Hall wave driven by the magnetic field line curvature. This result most closely matches our case with the thinnest region of resistivity η_z , where indeed reconnection is suppressed on the downstream side (with respect to the ion motion) but expands quickly upstream until it reaches the edge of the region with finite resistivity. However, our results show that in the kinetic case, reconnection proceeds differently when η_z is comparable to or

larger than the ion inertial length and when the current is largely carried by the ions. In that case it is the downstream side that has enhanced reconnection (see Figure 9, bottom panel, and Figure 11).

[40] To further illustrate this point, we show in Figure 13 the temporal evolution of the reconnected magnetic field B_x for the case $\eta_x = \eta_y = 4.0 c/\omega_{pi}$, $\eta_z = 1.0 c/\omega_{pi}$, and $\eta = 5 \times 10^{-5}$. For clarity, a box profile is used in the z -direction. Signatures are shown $3.0 c/\omega_{pi}$ along y away from the center. Apart from a small asymmetry, reconnection quickly proceeds on both sides (positive and negative z -direction) and fills out the available area of finite resistivity. Next, in Figure 14 we show an identical case, except here we widened the area of finite resistivity along z to $\eta_z = 4.0 c/\omega_{pi}$ at time $t = 10 \Omega_{ci}^{-1}$. The evolution of B_x is shown at three consecutive times in intervals of $2 \Omega_{ci}^{-1}$. Again, it is evident that reconnection quickly and homogeneously starts on both sides, with and against the current. There is no

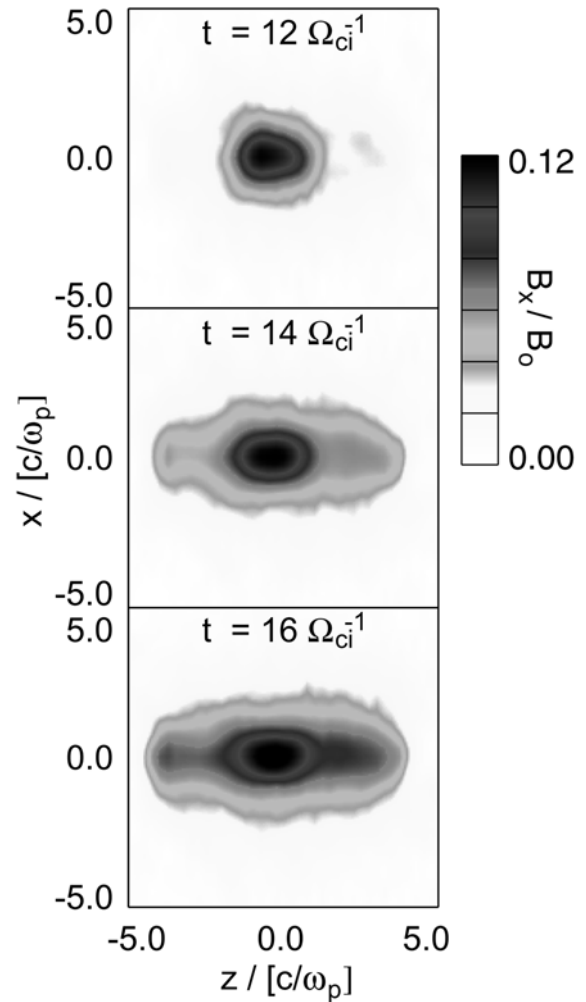


Figure 14. Evolution of the reconnection magnetic field B_x in 3-D hybrid simulations at three different times, as indicated, similar to Figure 13. Here, η_z is widened to $4.0 c/\omega_{pi}$ at time $t = 10 \Omega_{ci}^{-1}$. Again, reconnection quickly fills out the region with finite resistivity on both sides away from the center and does not propagate as a wave front against the current. See color version of this figure in the HTML.

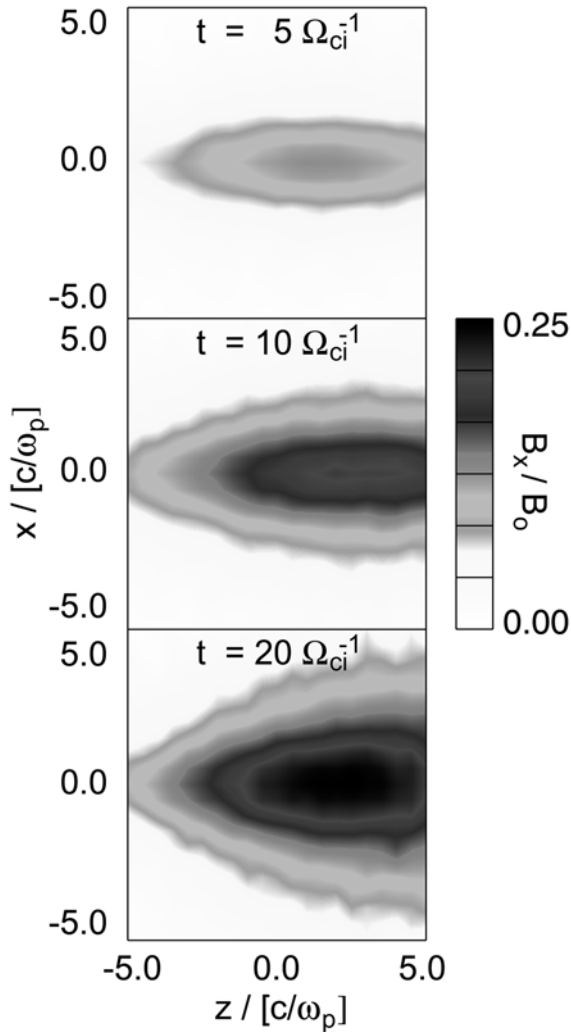


Figure 15. The $x - z$ cross section of the reconnected field B_x for $\eta_z = 4.0 c/\omega_{pi}$ in Hall-less 3-D hybrid simulations at three different times, as indicated. Cut taken $3 c/\omega_{pi}$ away from the center. As in the regular hybrid simulations shown in Figure 9, the ion flow enhances the reconnection signatures on the downstream side if the diffusion region is sufficiently wide in z . Thus this effect does not require the Hall term; instead, it is a consequence of the momentum associated with the current-carrying ions. See color version of this figure in the HTML.

evidence that it propagates as a wave front in either direction. As in our other hybrid simulations with sufficient width η_z , eventually, reconnection signatures are stronger on the downstream side.

3.6.2.3. 3-D Hall-less Hybrid Simulations

[41] For completeness we examine the above-documented asymmetry of these connection signatures when the Hall term is removed from the hybrid simulations. Similar to Figure 9, Figure 15 shows the $x - z$ cross section of the reconnected field B_x for $\eta_z = 4.0 c/\omega_{pi}$ ($\eta = 2 \times 10^{-4} c/\omega_{pi}$) in Hall-less 3-D hybrid simulations at three different times, as indicated. The cuts are taken $3 c/\omega_{pi}$ in y away from the center. As in the regular hybrid simulations displayed in Figure 9, the ion flow enhances the reconnection signatures on the downstream side if the diffusion region is sufficiently wide in z .

Thus as expected, this effect does not require the Hall term; instead, it is a consequence of the momentum associated with the current-carrying ions. Note that at late times, the asymmetry may be more pronounced at larger y -distances away from the center (cf. Figure 11) than at the $3 c/\omega_{pi}$ depicted here.

3.6.2.4. Reconnection Geometry in 3-D: Hybrid Simulations

[42] Finally, we remark on the question of reconnection geometry in three dimensions. In section 3.2 we demonstrated that in 2-D hybrid simulations, a relatively large η_y does not maintain a Sweet-Parker reconnection geometry. Instead, the configuration becomes unstable and appears to tend toward Petschek reconnection over time. Here, we discuss results from similar simulations in 3-D. The runs are slightly larger than our typical simulations above, with 100 by 200 by 100 cells, a cell size of $0.5 c/\omega_{pi}$, and ~ 60 million particles total. When we use a box profile with narrow extent in z ($\eta_x = 1.0 c/\omega_{pi}$, $\eta_y = 10.0 c/\omega_{pi}$, $\eta_z = 2.0 c/\omega_{pi}$, and $\eta = 4 \times 10^{-4}$), reconnection becomes unsteady at $\sim 20 \Omega_{ci}^{-1}$, with temporary X -points forming along y . However, over the time of the simulation ($40 \Omega_{ci}^{-1}$), the reconnection geometry simply remains unsteady but does not evolve from there. Comparing to the 2-D results, the question arises whether a reasonably fast evolution towards the Petschek configuration requires a sufficient extent of the diffusion region in z .

[43] In fact for the extreme case, i.e., homogeneous resistivity along z and periodic in z (infinite diffusion region extent in z), we find that the reconnection configuration indeed becomes unstable and reverts to Petschek reconnection in about $50 \Omega_{ci}^{-1}$, comparable to our 2-D simulations. Results are shown in Figure 16. This figure displays $x - y$ cross sections of the y -component of the velocity, normalized with the Alfvén velocity, and of the reconnected field

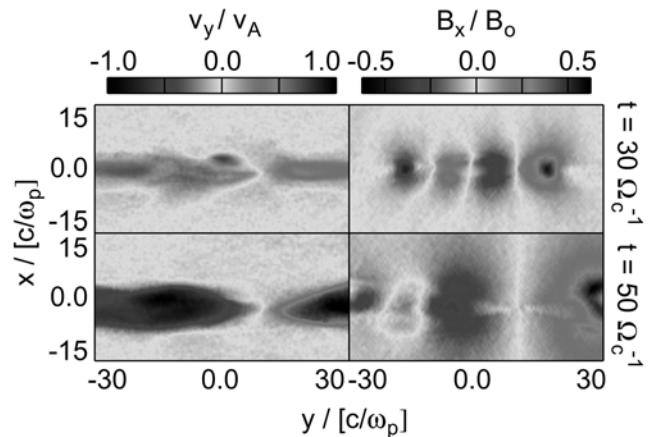


Figure 16. The $x - y$ cross sections of the normalized y -component of the velocity and of the reconnected field B_x in periodic 3-D hybrid simulations at two different times, as indicated. Resistivity is finite $\pm 10 c/\omega_{pi}$ around center in y , and $\pm 1 c/\omega_{pi}$ from center in x . Reconnection is slow at first in the Sweet-Parker configuration. At about 20 to $30 \Omega_{ci}^{-1}$ one of the edges of the Sweet-Parker domain starts to dominate, essentially leading to a Petschek-like configuration with much enhanced reconnection rate and Alfvénic outflow at about $50 \Omega_{ci}^{-1}$. See color version of this figure in the HTML.

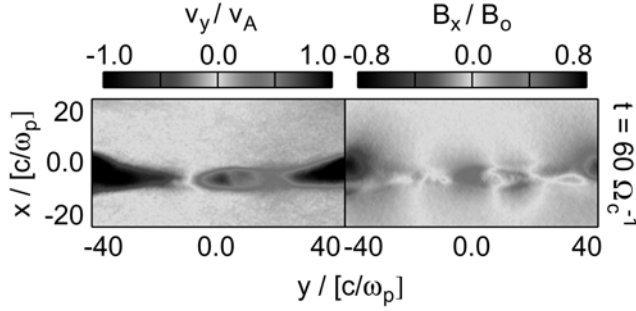


Figure 17. The $x - y$ cross sections of the normalized y -component of the velocity and of the reconnected field B_x in a nonperiodic 3-D hybrid simulation. Resistivity has the box shape with $\pm 10 c/\omega_{pi}$ around center in y , $\pm 1 c/\omega_{pi}$ from center in x , and $\eta_z = 8 c/\omega_{pi}$ in z with a cosh profile. Similar to the periodic run with homogeneous resistivity along z shown in Figure 16, the Sweet-Parker configuration becomes unstable and tends toward Petschek at about $60 \Omega_{ci}^{-1}$. At this point in time, a growing kink instability has started to shift the current layer outside the region of resistivity, starting to suppress further reconnection. See color version of this figure in the HTML.

B_x at two different times, as indicated. Resistivity is finite at $\pm 10 c/\omega_{pi}$ around the center in y , and $\pm 1 c/\omega_{pi}$ from the center in x . Reconnection is slow at first in the Sweet-Parker configuration. At $\sim 20 - 30 \Omega_{ci}^{-1}$ one of the edges of the Sweet-Parker domain starts to dominate, essentially leading to a Petschek-like configuration with much enhanced reconnection rate and Alfvénic outflow at $\sim 50 \Omega_{ci}^{-1}$. Note that the outflow velocity doubles between the two time frames shown. There is also a small-amplitude ion-ion kink instability [Karimabadi et al., 2003b; Karimabadi et al., 2003a] that develops at about the same time. The instability shifts the current sheet slightly away from the x -center of the simulation box but does not appear to interfere otherwise with the reconnection up to this point.

[44] In a series of nonperiodic simulations with a box profile in x and y , $\eta_x = 1.0 c/\omega_{pi}$, $\eta_y = 10.0 c/\omega_{pi}$, $\eta = 4 \times 10^{-4}$, and varying η_z (cosh profile), the y -extended reconnection region becomes unstable and reverts to Petschek reconnection within the duration of our typical simulations ($40 \Omega_{ci}^{-1}$ to $80 \Omega_{ci}^{-1}$) at $\eta_z \sim 8.0 c/\omega_{pi}$. Figure 17 shows the y -component of the velocity and of the reconnected field B_x in a similar format as Figure 16, at $60 \Omega_{ci}^{-1}$, $3.0 c/\omega_{pi}$ downstream from the z -center. Again, reconnection at one edge of the Sweet-Parker diffusion region starts to dominate. However, in this case the ion-ion kink mode has grown to amplitudes so as to shift the current layer sufficiently away from the diffusion region, interfering with further reconnection. We would also like to note that as in our other nonperiodic simulations, reconnection is at this value of η_z still distinctly three-dimensional, with different reconnection signatures as a function of z .

[45] Since we cannot run the simulations arbitrarily long, and given the interference of the kink mode, the above value of $\eta_z \sim 8.0 c/\omega_{pi}$ is just an upper limit. In other words, based on the ion physics alone, given sufficient time and in 3-D, a Sweet-Parker type reconnection region will likely convert to a Petschek reconnection configuration for most values of η_z

of interest. In a limited number of runs with varying η_x and η_y , and also using the cosh resistivity profile, we find that the time scale over which an initial Sweet-Parker configuration becomes unstable depends on the geometric shape of the diffusion region.

4. Discussion and Summary

[46] In this paper we addressed several interrelated issues regarding the process of magnetic reconnection in a kinetic plasma. The main results are summarized below.

4.1. Sweet-Parker Versus Petschek Reconnection

[47] There has been a strong interest in understanding the conditions under which different reconnection regimes, Sweet-Parker versus Petschek, are realized. Studies based on MHD have shown [Ugai and Tsuda, 1977; Scholer, 1989; Yan et al., 1992; Ugai, 1999] that Sweet-Parker reconnection is obtained unless the resistivity is localized in a small region. Here we reexamined this issue in the kinetic regime. We found significant differences with MHD results. First, in MHD, the region where resistivity is imposed coincides with the diffusion region, so the observed link between the size of the resistive region and the rate of reconnection is not too surprising. However, we have shown here that in a kinetic plasma the size of the diffusion region is in general different than the size of the localized resistivity. This is because the main role of resistivity is as a reconnection enabler by breaking the frozen-in condition. However, the long time evolution of the system is dominated by ion physics and is not tied to the resistive scales. Second, we find that Sweet-Parker reconnection is not a stationary solution for physically interesting forms and sizes of the resistivity region. In MHD, since there are no intrinsic scales, one has the freedom to consider an arbitrary range in δ/Δ , where δ is the resistivity-dependent width of the diffusion region and Δ is the length of the diffusion region along the outflow direction. In a real system, however, there are physical scales and this limits the range in δ/Δ . For example, in the magnetotail, one ion inertial length is $\sim 1/6$ th of Earth radius, so it would be unrealistic to consider Δ of 100 ion inertial lengths in the magnetotail or assume that the resistivity would be uniform over such a large region in space. Taking this physical reality into account, we considered the conditions under which Sweet-Parker and Petschek reconnection maybe obtained in a kinetic plasma. We found that under certain conditions the system initially can evolve based on the Sweet-Parker scenario, but this is not a stable configuration and, given enough time, the system becomes unstable and evolves toward a Petschek reconnection. Furthermore, the requirement of uniform resistivity over many ion inertial lengths for the initial evolution to Sweet-Parker reconnection is not likely to be realized in a real plasma. Thus it seems unlikely that Sweet-Parker reconnection would occur in the magnetosphere, although it may occur in other physical settings where ion inertial length is very small compared with other relevant parameters.

4.2. Role of System Size on Magnetic Reconnection

[48] We showed that as long as the system size is much longer than the ion inertial length c/ω_{pi} , the details of reconnection become independent of the system size. This

kinetic result is in agreement with the results of *Shay et al.* [1999, 2004] that showed that reconnection remains Alfvénic in a collisionless plasma even when the macroscopic scale length of the system becomes large, with a reconnection rate that is independent of the system size. Additionally, the recent work of *Huba and Rudakov* [2004] demonstrated that the asymptotic (i.e., time-independent) state of a reversed-field configuration is nearly independent of the initial current sheet width. Specifically, the Hall reconnection rate is weakly dependent on the initial current layer width and is $\partial\Phi/\partial t \lesssim 0.1 V_{A0}B_0$, where V_{A0} is the Alfvén velocity and B_0 is the magnetic field strength in the upstream region. Moreover, this rate appears to be independent of the scale length on which the electron “frozen-in” condition is broken (as long as it is $< c/\omega_{pe}$).

4.3. Possibility of Fast Reconnection Due to Ion Kinetics

[49] GEM challenge studies *Birn et al.*, 2001; *Kuznetsova et al.*, 2001] bypassed the initial linear growth phase of the current sheet by imposing a rather large external perturbation and calculated the reconnection rate and compared it between MHD, Hall MHD, hybrid, and full particle simulations. Since periodic simulations (in the direction along the initial magnetic field) were used, the system did not reach steady state and therefore connection rate was time-dependent. It was found that reconnection rate is insensitive to the details of how the frozen-in condition is broken and found similar rates in Hall MHD, hybrid, and full particle simulations but found much lower reconnection rate in MHD. Fast reconnection and its absence in MHD was explained in terms of the quadratic dispersion property of whistlers (higher phase speed at smaller spatial scales). We took a different approach and used simulations with inflow-out flow boundary conditions, allowing the system to reach steady state, and then compared the value of the reconnection rate between the hybrid and Hall-less hybrid simulations. Since whistlers are dispersionless in the Hall-less hybrid case (e.g., Figure 2), we also tested the connection between whistler dispersion and fast reconnection, as suggested by GEM challenge studies. We found that the asymptotic reconnection rate is very similar in both cases and is $\sim 0.15 V_{A0}B_0$. This clearly demonstrates two very important points: (1) ion kinetic alone, and even in the absence of the Hall term, can give rise to fast reconnection and (2) quadratic property of whistlers is not critical to fast reconnection in the kinetic regime.

4.4. 3-D Asymmetries and Reconnection Waves

[50] Three-dimensional Hall-MHD simulations of reconnection have revealed the presence of asymmetries in the magnetic field [*Huba and Rudakov*, 2002; *Shay et al.*, 2003]. We provided a physical picture for these so-called reconnection waves and examined their possibility in the kinetic regime. We found marked differences between Hall MHD and hybrid results in the nature of asymmetry arising due to the third dimension. In Hall MHD the asymmetry propagates as a wave in the direction of the flow of the current-carrying population [*Huba and Rudakov*, 2002; *Shay et al.*, 2003]. In the case where the electrons are current-carriers, then the reconnection wave would propagate in the direction of the electrons. In 3-D hybrid,

however, the observed asymmetry is simply due to ion flow (including a time-of-flight effect) rather than a propagating wavefront. The observed asymmetries in the magnetic field arising in 3-D Hall-MHD simulations of reconnection [*Huba and Rudakov*, 2002; *Shay et al.*, 2003] are eliminated in the kinetic regime due to dominance of ion flows. One exception is for very thin resistive layers in the third dimension where the results of *Huba and Rudakov* [2002] are obtained. These results clearly demonstrate the importance of ion kinetic effects in the reconnection process for ion scale current layers.

[51] The absence of the reconnection wave in the kinetic regime needs further clarification. In Hall MHD simulations of the reconnection wave, including the one shown here in Figure 10, the equilibrium current is carried by the electrons and the reconnection wave moves in the direction of the electrons. *Shay et al.* [2003] suggested that if the current/flow were to be carried by the ions, the reconnection wave would then move in the direction of the ions. In our hybrid simulations the ions carry the bulk of the current as in the magnetotail, but unlike in Hall MHD, there is no evidence that the enhanced reconnection propagates as a wave front in either direction. Although we have not performed any hybrid simulations where the electrons are the dominant current carriers, in practice it is the ions that typically carry most of the equilibrium current in the magnetotail or at the magnetopause. One possible exception may be in the thin current layers that are at times observed embedded within a thicker current layer in the magnetotail. The current within such thin layers would be carried by the electrons, whereas the overall current of the thicker sheet would be carried by the ions. The possibility of reconnection waves in such double structured sheets remains an interesting open question.

[52] The above results are relevant to the magnetotail where dawn-dusk asymmetries are observed in the motions of auroral brightenings and surges, as well as in the statistical location of pressure decreases, flows, and magnetic signatures associated with the near-Earth neutral line and early plasmoids [*Ieda et al.*, 1998; *Miyashita et al.*, 2000; *Raj et al.*, 2002]. We have shown that 3-D reconnection is inherently asymmetric; in Hall MHD the asymmetry is caused by a reconnection wave (Figure 10), while in the kinetic regime it is caused by ion flow (Figure 11). Given that ions carry the bulk of the current in the magnetotail, we expect that observed asymmetries are due to ion flows in three-dimensional reconnection rather than an electron-driven reconnection wave [see also *Krauss-Varban et al.*, 1999b]. Detailed comparison with observations will be discussed in a future publication.

[53] One area for future work would be to have a fluid code that has both the Hall and an anisotropic ion pressure tensor (e.g., finite Larmor radius effects). Such a code and its comparison with the hybrid and Hall-less hybrid simulations would facilitate a better understanding of the details of the kinetic ion physics that seem to dominate the reconnection process.

Appendix A

[54] For simulations that involve magnetic diffusion and “out-of-plane” magnetic field generation, it is advisable to

evaluate available numerical algorithm(s) for accuracy and stability. Hybrid codes have been around for more than 30 years [Harned, 1982; Winske, 1985]. While from a mathematical viewpoint, they may not be quite as well understood as comparable fluid algorithms, much experience has been gained over this time concerning their numerical properties. In recent years the vast majority of published computations have used one of three distinct types of codes: a direct solver (one-pass method [Thomas *et al.*, 1990; Fujimoto, 1990; Omidi *et al.*, 2001]), the predictor-corrector scheme [Harned, 1982; Quest, 1989], and an algorithm based on a moment method [Quest, 1989; Matthews, 1994]. The history and details of hybrid codes are further detailed in the works of Omidi *et al.* [2001] and Winske *et al.* [2003].

[55] It is quite straightforward to understand what distinguishes the above approaches to hybrid algorithms. The codes used in any significant number of application to date employ, like most particle simulations, a leapfrog method to advance the spatial and velocity components of the pseudo-particles. This means that the spatial positions and velocities are calculated on a temporal grid 1/2 time step apart. From this, moments of the ion (charge) density and currents are obtained to allow calculation of the electric and magnetic field.

[56] The magnetic field is simply advanced from Faraday's law (equation (3)), only involving the electric field as a source at a certain, defined time step. As can be seen from equation (2) in the main text of this paper, the electric field is derived from the electron momentum equation (Ohm's law) and is a state equation. This means that results for \mathbf{E} can be obtained without time advance from a given set of sources (density n , ion velocity/current \mathbf{v}/\mathbf{J} , and magnetic field \mathbf{B}) and at a certain time. The most important point here is to realize that due to the use of a leapfrog method for the particles, the two desired source quantities (n , \mathbf{v}) will not be available at the same said time step to solve for \mathbf{E} . Further, advancing \mathbf{B} in any scheme that is more accurate and more stable than simple forward differencing requires knowledge of an approximation to \mathbf{E} at a later time that is yet to be calculated (and that implicitly involves \mathbf{B} and the moments at this later time). Conversely, calculation of the moments at such advanced times may require pushing the particles using \mathbf{E} and \mathbf{B} at advanced times. Hybrid codes differ in their approach on how to remedy this interdependence in a stable, accurate, and fast way.

[57] In addition, stability, accuracy, and conservation properties may be affected by the positions at which the velocity moments are collected. We will elaborate on this further below.

[58] The basic codes mentioned above are described in detail in the literature. For here, it suffices to summarize their general guiding principles; see Figure A1 for a sketch of a simple explicit solver (Figure A1a) and a predictor corrector scheme (Figure A1b). The direct solve (one-pass method) tries to avoid a second particle push to align the sources for \mathbf{E} . Instead, it uses an extrapolation of the velocities when calculating \mathbf{E} . For this reason, it is a relatively fast algorithm.

[59] The predictor-corrector scheme is known for its accuracy in describing the shorter wavelength/higher fre-

quency portion of the wave spectrum. It consists of a two-step process, in which an extrapolated value of \mathbf{E} is used to advance a temporary \mathbf{B} and to move the particles for a second moment collect, while a corrector step ensures accurate sources for the final \mathbf{E} calculation, maintaining a time-centered philosophy. Although slower than the direct-solve method for a given time step, its CPU time typically competes well at any defined required level of accuracy.

[60] The CAM-CL method, as developed by Matthews [1994], avoids the second particle push by employing a moment method as in earlier variations of the hybrid code [Quest, 1989]. The equations involved are somewhat cumbersome, but in the end there is little overhead compared with the one-pass method.

[61] When extrapolating the velocity moments to match the desired point in time, one can involve higher-order schemes to accomplish this [Fujimoto, 1990; Thomas *et al.*, 1990]. However, in extensive tests and comparisons, we have found no advantage of doing so. Thus we only report here on using linear extrapolation/interpolation in the moments for both the proper time slice evaluation and for evaluating moments within substepping.

[62] Finally, for very high frequency/short wavelength waves, one can make the argument that typically, only modes that are almost field-aligned are not heavily damped and thus contribute to the physical and numerical properties of the simulation. These modes do not involve significant perturbations of the density and velocity components. As such, it is advantageous to substep the electric field solver and magnetic field advance without recalculating the particle sources [Swift, 1995; Matthews, 1994]. Here, we use a Runge-Kutta [Press *et al.*, 1992] scheme for this substepping in the one-pass and CAM-CL codes. Moreover, the Runge-Kutta scheme is generally used in our one-pass algorithm instead of the two-step explicit process indicated in Figure A1a. In the predictor-corrector code it is more practical to continue the predictor-corrector scheme on a substep basis, which is what we do. The particle push/moment collect indicated in steps 1, 2, and 6 of Figure A1b are then only executed in the first and last substep, respectively. In this code, moments are interpolated/extrapolated as needed for other substep points. As a guideline, we find that for typical plasma parameters and numbers of particles per cell, substepping beyond 4 to 16 per regular time step is commonly less efficient than using a smaller time step for the entire computation. The exact number depends on the cost of the particle push compared with the field solve (i.e., on the number of particles per cell and on field solver overhead incurred during parallel processing). Also, using a large number of substeps at a relatively large time step can lead to numerical instability.

[63] Coming back to the question of at what particle position the velocity moments should be evaluated, there are two competing principles. Standard practice (method 1) is to honor the fact that the velocities are evaluated 1/2 temporal step before the positions and thus to use particle positions for the \mathbf{v} moment evaluation at this time. A simpler method (method 2) uses the particle positions that are more readily available, namely, 1/2 half step farther advanced, after the particle positions have been updated, and thus at the same time the density moment is collected. It turns out that method 2 is susceptible to an instability

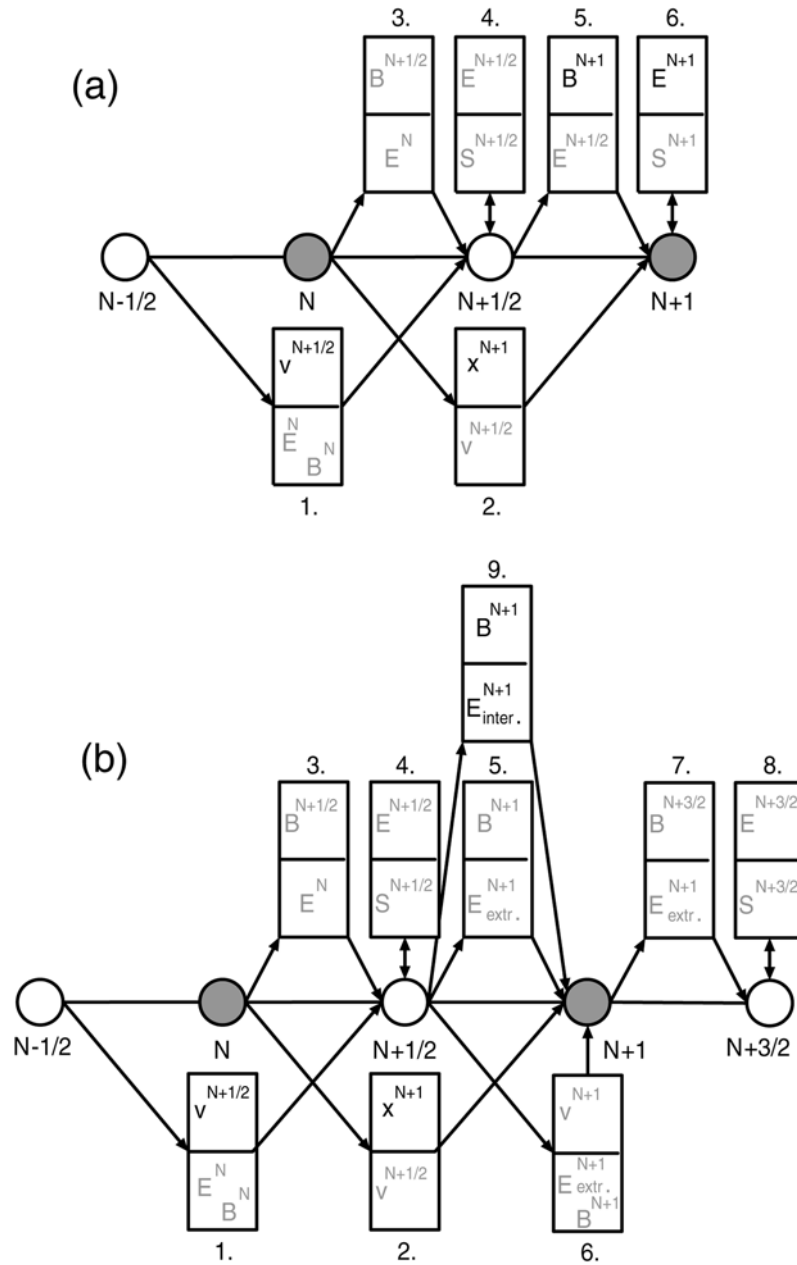


Figure A1. Flow charts of (a) a simple explicit hybrid algorithm and (b) a predictor-corrector version. Black letters indicate permanent solution; gray letters denote temporary values. The top of each box shows the calculated quantity; the bottom shows its sources. S stands for the magnetic field, density, and ion velocity sources combined. Our one-pass method is loosely based on the first algorithm, except that a Runge-Kutta method with arbitrary substepping is used instead of the two-step, explicit method indicated. Because of the symmetry between forward and backward differences when calculating B, steps 5, 7, and 9 of the predictor-corrector algorithm are effectively time-centered.

transverse to **B** reminiscent of mirror waves under certain parameter combinations (e.g., when the density is low and the magnetic field is large, as for example in the magnetosphere). On the other hand, method 1 in some algorithms leads to artificial particle heating when the streaming velocity of the plasma is large compared with the thermal velocity, unless a very small time step is chosen. We will report on details of these numerical effects elsewhere.

[64] To resolve the numerical challenges outlined above, we employ a method based on the local and instantaneous

Courant-Friedrich-Levy (CFL) condition of the particle (the ratio of its spatial advance in one time step compared with the cell size) in the one-pass algorithm. In other words a particle that is fast in a particular direction is evaluated using method 2, whereas a slow-moving particle uses method 1. We were not able to employ such a method in the CAM-CL algorithm, which in its moment prediction uses method 1 by default. In our tests the predictor-corrector algorithm does not require this modification and works best with method 1.

[65] We find that for most practical circumstances, any of the above three codes give excellent results. A typical example is shown in Table A1. Here, we tested the magnetic field fluctuations and heating associated with plasma discontinuities moving at a moderate speed of $V_A/2$. The 2-D simulation box (100×100 cells, cell size $0.5 c/\omega_{pi}$) was divided into a high proton beta plasma ($\beta_p = 2.0$) and a low beta plasma (density $1/4$, proton temperature $1/8$, magnetic field ~ 1.7 of high β region) with two distinct, pressure-balanced ion populations and small electron temperature equal to the proton temperature of the cold region throughout. The field fluctuations and temperatures of this test gave similar results; only the perpendicular temperature of the colder species is reported here, at the end of the simulation (16,000 steps at smallest time step). Owing to the small density in the low beta region, the CFL condition on the whistler waves requires $\Delta t \lesssim 0.02 \Omega_{ci}^{-1}$. Indeed, we find that the unmodified one-pass and predictor-corrector codes are unstable for $\Delta t = 0.04 \Omega_{ci}^{-1}$. The fact that the CAM-CL code is still stable at that time step, as well as its lower temperature results in Table A1, indicate that it is slightly diffusive. For example, with finite background resistivity and/or smoothing of the sources, the other two codes also run stable for $\Delta t = 0.04 \Omega_{ci}^{-1}$ but with the consequence of associated numerical cooling. That is, artificial removal of the highest mode number waves typically leads to cooling of the plasma. There are other methods to avoid the limit posed by the CFL condition on the whistlers, without excessive numerical cooling. We will report on one such method elsewhere.

[66] We have not found any significant differences concerning the out-of-plane magnetic field or other important plasma parameters, when run at a sufficiently small time step. Differences between the codes surface in challenging situations, where convergence at the least amount of CPU time is important and sought after.

[67] For example, regardless of our comments when discussing Table A1, all three algorithms have negligible numerical diffusion/resistivity under common circumstances. Even very thin current sheets with thickness small compared with the ion inertial length will not reconnect unless resistivity is (locally) added, breaking the frozen-in condition for the electrons. However, in antiparallel magnetic field configurations embedded in streaming plasmas, numerical diffusion is present and reconnection may occur. In this case we found that the CAM-CL code has by far the largest amount of diffusion, followed by the one-pass method, with the predictor-corrector being the least diffusive. Results are shown in Table A2 for a plasma config-

Table A1. Normalized Ion Temperature of a Cold Species Surrounded By a Hot Species in Periodic Simulations (See Text For Details)^a

Time Step, Ω_{ci}^{-1}	0.02	0.01	0.005
Predictor-corrector	0.6058	0.6040	0.6082
One-pass	0.6277	0.6078	0.6110
CAM-CL	0.5953	0.6040	0.6114

^aResults for the three codes, as indicated, are shown for various time steps. All codes demonstrate acceptable results at a time step of $0.01 \Omega_{ci}^{-1}$, for this problem (double precision would be required to make further distinctions, for this specific problem).

Table A2. Normalized Ion Temperature of a Cold Species Surrounded By a Hot Species in Periodic Simulations With Antiparallel Fields and Fast, Streaming Plasma (See Text For Details)^a

Time Step, Ω_{ci}^{-1}	0.01	0.005	0.0025
Predictor-corrector	0.16193 moderate	0.9663 slight	0.9366 none
One-pass	0.55176 severe	0.21764 moderate	0.19279 moderate
CAM-CL	0.38723 severe	0.22560 severe	0.19820 severe

^aResults for the three codes, as indicated, are shown for various time steps. Additional verbiage indicates severity of numerical diffusion/reconnection in streaming plasma.

uration similar to that described for the test case of Table A1, except with antiparallel magnetic fields, $1/2$ the cell size, and a streaming velocity of $8 V_A$ (typical solar wind speed at 1AU), run up to 32,000 time steps. Here, “slight” reconnection means that there is no consequence on the temperatures of the plasma components, “moderate” means that the low-temperature plasma is significantly heated, and “severe” means that both plasma components are significantly heated. In agreement with the conjectures concerning numerical diffusion in the three codes drawn above, we find that the CAM-CL code is not very suitable to applications in a moving plasma, while the predictor-corrector method behaves the best under challenging circumstances.

[68] While the predictor-corrector algorithm uses more CPU time due to its second particle advance, when implemented as indicated in Figure A1b (only the \mathbf{v} -moments are evaluated a second time, not n), it is only $\sim 20\%$ slower than the one-pass method under typical circumstances. Evaluating \mathbf{v} at $N + 1$ rather than the conventional $N + 3/2$ allows us to subsequently calculate interpolated values in the substepping process. In practice, to preserve the nonlinear properties of the particle push, this is done by advancing to $N + 3/2$ and then dividing the advance by two. Extrapolation to $N + 3/2$ then simply recovers the full step.

[69] To summarize, the one-pass method is simple, accurate, and efficient, and we use it as a standard code. Under circumstances where high accuracy and best conservation properties are required, eventually, the predictor-corrector method outshines the one-pass scheme.

[70] **Acknowledgments.** The research of H. Karimabadi, D. Krauss-Varban, and H. X. Vu was supported by NASA SEC Theory Program NAG5-11754 and NSF grant ATM-9901665. The hybrid simulations were performed at the local NASHI PC cluster and the San Diego Supercomputer Center, which is supported by the National Science Foundation. The research of J. D. Huba was supported by NASA and ONR. We thank K. Quest, N. Omid, M. Shay, and P. Pritchett for valuable discussions.

[71] Shadia Rifai Habbal thanks Maria M. Kuznetsova and another referee for their assistance in evaluating this paper.

References

- Birn, J., et al. (2001), Geospace environmental modeling (GEM) magnetic reconnection challenge, *J. Geophys. Res.*, *106*, 3715.
 Biskamp, D., and E. Schwarz (2001), Localization, the clue to fast magnetic reconnection, *Phys. Plasmas*, *8*, 4729.
 Dungey, J. W. (1961), Interplanetary magnetic field and the auroral zones, *Phys. Rev. Lett.*, *6*, 47.
 Erkaev, N. V., V. Semenov, and F. Jamitzky (2000), Reconnection rate for the inhomogeneous resistivity Petschek model, *Phys. Rev. Lett.*, *84*, 1455.

- Fujimoto, M. (1990), Instabilities in the magnetopause velocity shear layer, Ph.D. thesis, Univ. of Tokyo, Tokyo.
- Hain, K. (1987), The parital donor cell method, *J. Comput. Phys.*, *73*, 131.
- Harned, D. S. (1982), Quasineutral hybrid simulation of macroscopic plasma phenomena, *J. Comp. Phys.*, *47*, 452.
- Huba, J. D. (1991), Theory and simulation of a high-frequency magnetic drift wave, *Phys. Fluids B*, *3*, 3217.
- Huba, J. D. (2003), A tutorial on Hall magnetohydrodynamics, in *Space Plasma Simulation*, edited by J. Büchner, C. T. Dum, and M. Scholer, p. 170, Springer-Verlag, New York.
- Huba, J. D., and J. G. Lyon (1999), A new 3D MHD algorithm: The distribution function method, *J. Plasma Phys.*, *61*, 391.
- Huba, J. D., and L. I. Rudakov (2002), Three dimensional Hall magnetic reconnection, *Phys. Plasmas*, *9*, 4435.
- Huba, J. D., and L. I. Rudakov (2004), The Hall magnetic reconnection rate, *Phys. Rev. Lett.*, in press.
- Ieda, A., S. Machida, T. Mukai, Y. Saito, T. Yamamoto, A. Nishida, T. Terasawa, and S. Kokubun (1998), Statistical analysis of the plasmoid evolution with Geotail observations, *J. Geophys. Res.*, *103*, 4453.
- Ji, H., M. Yamada, S. Hsu, R. Kulsrud, T. Carter, and S. Zaharia (1999), Magnetic reconnection with Sweet-Parker characteristics in two-dimensional laboratory plasmas, *Phys. Plasmas*, *6*, 1743.
- Karimabadi, H., D. Krauss-Varban, N. Omidi, and H. X. Vu (1999), Magnetic structure of the reconnection layer and core field generation in plasmoids, *J. Geophys. Res.*, *104*, 12,313.
- Karimabadi, H., P. L. Pritchett, W. Daughton, and D. Krauss-Varban (2003a), Ion-ion kink instability in the magnetotail: 2. Three-dimensional full particle and hybrid simulations and comparison with observations, *J. Geophys. Res.*, *108*(A11), 1401, doi:10.1029/2003JA010109.
- Karimabadi, H., W. Daughton, P. L. Pritchett, and D. Krauss-Varban (2003b), Ion-ion kink instability in the magnetotail: 1. Linear theory, *J. Geophys. Res.*, *108*(A11), 1400, doi:10.1029/2003JA010026.
- Karimabadi, H., J. Huba, D. Krauss-Varban, and N. Omidi (2004), On the generation and structure of the quadrupole magnetic field in the reconnection process: Comparative simulation study, *Geophys. Res. Lett.*, *31*, L07806, doi:10.1029/2004GL019553.
- Krauss-Varban, D., and H. Karimabadi (2003), Timing and localization of reconnection signatures—Is there a substorm model problem?, *Geophys. Res. Lett.*, *30*(6), 1308, doi:10.1029/2002GL016369.
- Krauss-Varban, D., H. Karimabadi, and N. Omidi (1999a), Two-dimensional structure of the co-planar and non-coplanar magnetopause transition during reconnection, *Geophys. Res. Lett.*, *26*, 1235.
- Krauss-Varban, D., N. Omidi, and K. B. Quest (1999b), Three-dimensional simulations of reconnection onset: Ion-kinetic tail processes and ionospheric signatures, *Eos Trans. AGU*, *80*(46), Fall Meet. Suppl., 880.
- Kuznetsova, M. M., M. Hesse, and D. Winske (2001), Collisionless reconnection supported by nongyrotropic pressure effects in hybrid and particle simulations, *J. Geophys. Res.*, *106*, 3799.
- Mandt, M. E., R. E. Denton, and J. F. Drake (1994), Transition to whistler mediated magnetic reconnection, *Geophys. Res. Lett.*, *21*, 73.
- Matthews, A. P. (1994), Current advance method and cyclic leapfrog for 2-D multispecies hybrid plasma simulations, *J. Comp. Phys.*, *112*, 102.
- Miyashita, Y., S. Machida, T. Mukai, Y. Saito, K. Tsuruda, H. Hayakawa, and P. R. Sutcliffe (2000), A statistical study of variations in the near and mid-distant magnetotail associated with substorm onset: GEOTAIL observations, *J. Geophys. Res.*, *105*, 15,913.
- Omidi, N., H. Karimabadi, and K. B. Quest (2001), Global hybrid simulations of solar wind interaction with the magnetosphere, paper presented at the Sixth International School/Symposium for Space Plasma Simulations, Copernicus Gesellschaft, Garching, Germany.
- Parker, E. N. (1957), Sweet's mechanism for merging magnetic field in conducting fluids, *J. Geophys. Res.*, *62*, 509.
- Petschek, H. E. (1964), Magnetic field annihilation, in *AAS-NASA Symposium on the Physics of Solar Flares*, Spec. Publ. SP-50, p. 425, NASA, Washington, D. C.
- Press, W. H., B. P. Flannery, S. A. Teukolsky, and W. T. Vetterling (1992), *Numerical Recipes in FORTRAN: The Art of Scientific Computing*, 2nd ed., Cambridge Univ. Press, New York.
- Pritchett, P. L. (2001), Geospace environment modeling magnetic reconnection challenge: Simulations with a full particle electromagnetic code, *J. Geophys. Res.*, *106*, 3783.
- Quest, K. B. (1989), Hybrid simulation, in *The 3rd International School for Space Simulation (ISSS-3): Tutorial Courses*, edited by B. Lembge, pp. 172–182, Copernicus Gesellschaft, Garching, Germany.
- Raj, A., T. Phan, R. P. Lin, and V. Angelopoulos (2002), Wind survey of high-speed bulk flows and field-aligned beams in the near-Earth plasma sheet, *J. Geophys. Res.*, *107*(A12), 1419, doi:10.1029/2001JA007547.
- Scholer, M. (1989), Undriven magnetic reconnection in an isolated current sheet, *J. Geophys. Res.*, *94*, 8805.
- Shay, M. A., J. F. Drake, B. N. Rogers, and R. E. Denton (1999), The scaling of collisionless, magnetic reconnection for large systems, *Geophys. Res. Lett.*, *26*, 2163.
- Shay, M. A., J. F. Drake, B. N. Rogers, and R. E. Denton (2001), Alfvénic collisionless magnetic reconnection and the Hall term, scaling of collisionless, magnetic reconnection for large systems, *J. Geophys. Res.*, *106*, 3759.
- Shay, M. A., J. F. Drake, M. Swisdak, W. Dorland, and B. N. Rogers (2003), Inherently three dimensional magnetic reconnection: A mechanism for bursty bulk flows?, *Geophys. Res. Lett.*, *30*(6), 1345, doi:10.1029/2002GL016267.
- Shay, M. A., J. F. Drake, M. Swisdak, and B. N. Rogers (2004), The scaling of embedded collisionless reconnection, *Phys. Plasmas*, *11*(5), 2199.
- Sonnerup, B. U. O. (1979), Magnetic field reconnection, in *Solar System Plasma Physics*, edited by L. J. Lanzerotti, C. F. Kennel, and E. N. Parker, p. 46, North-Holland, New York.
- Sweet, P. A. (1958), The neutral point theory of solar flares, in *Electromagnetic Phenomena in Cosmic Physics*, edited by B. Lehnert, p. 135, Cambridge Univ. Press, New York.
- Swift, D. (1995), Use of a hybrid code to model the Earth's magnetosphere, *Geophys. Res. Lett.*, *22*, 311.
- Terasawa, T. (1983), Hall current effect on tearing mode instability, *Geophys. Res. Lett.*, *10*, 475.
- Thomas, V. A., D. Winske, and N. Omidi (1990), Reforming supercritical quasi-parallel shocks: 1. One- and two-dimensional simulations, *J. Geophys. Res.*, *95*, 18,809.
- Ugai, M. (1999), Computer studies on the spontaneous fast reconnection model as a nonlinear instability, *Phys. Plasmas*, *6*, 1522.
- Ugai, M., and T. Tsuda (1977), Magnetic field line reconnection by localized enhancement of resistivity, 1, Evolution in a compressible MHD fluid, *J. Plasma Phys.*, *17*, 337.
- Uzdensky, D. A., R. M. Kulsrud, and M. Yamada (1996), Theoretical analysis of driven magnetic reconnection experiments, *Phys. Plasmas*, *3*, 1220.
- Vasyliunas, V. M. (1975), Theoretical models of magnetic field line merging, 1, *Rev. Geophys.*, *13*, 303.
- Winske, D. (1985), Hybrid simulation codes with application to shocks and upstream waves, *Space Sci. Rev.*, *42*, 53.
- Winske, D., L. Yin, N. Omidi, H. Karimabadi, and K. B. Quest (2003), Hybrid simulation codes: Past, present and future: Tutorial, in *Space Plasma Simulations, Lecture Notes in Phys.*, vol. 615, edited by J. Buechner, C. T. Dum, and M. Scholer, p. 359, Springer-Verlag, New York.
- Yan, M., L. C. Lee, and E. R. Priest (1992), Fast magnetic reconnection with small shock angles, *J. Geophys. Res.*, *97*, 8277.
- Yokokawa, N., M. Fujimoto, Y. Yamada, and T. Mukai (2001), Hall effects on field-aligned current generation in three-dimensional magnetic reconnection, *Earth Planets Space*, *53*, 501.

J. D. Huba, Naval Research Laboratory, Code 6790, Washington, DC 20375, USA.

H. Karimabadi, D. Krauss-Varban, and H. X. Vu, Department of Electrical and Computer Engineering, University of California, San Diego, 9500 Gilman Drive, La Jolla, CA 92093-0407, USA. (homa@ece.uscd.edu)